Chemical Geology 635 (2023) 121618

Contents lists available at ScienceDirect

Chemical Geology

journal homepage: www.elsevier.com/locate/chemgeo

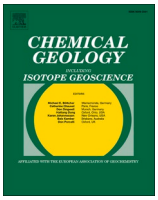

Greigite formation in aqueous solutions: Critical constraints into the role of iron and sulphur ratios, pH and Eh, and temperature using reaction pathway modelling

Jack N. Turney *, Dominik Weiss, Adrian R. Muxworthy, Alastair Fraser

Department of Earth Sciences and Engineering, Imperial College London, London, UK

ARTICLE INFO

Editor: Karen Johannesson

Keywords:
Greigite
iron sulphides
Aqueous solutions
Reaction pathway modelling
Mackinawite
Pyrite

ABSTRACT

Greigite forms as an intermediate phase along the pyrite reaction pathway. Despite being considered metastable, it is observed in numerous shallow natural systems, suggesting it could be a unique proxy for diagenetic and environmental conditions. We use thermodynamic reaction pathway modelling in PHREEQC software, to understand the role of iron and sulphur ratios, pH and Eh, and temperature on the formation and retention of greigite in aqueous solutions. With newly available experimental thermodynamic properties, this work identifies the chemical boundary conditions for greigite formation in aqueous solutions. Greigite precipitation is likely favourable in anoxic and alkaline aqueous solutions at or below 25 °C. Our numerical experiments show that greigite is closer to saturation in iron-rich solutions with minor sulphur input. Greigite precipitation in strongly alkaline solutions suggest polysulfides and ferric iron-bearing minerals may be favourable reactants for its formation. Greigite precipitates at iron and sulphur concentrations that are over two orders of magnitude greater than iron sulphide-hosted natural porewaters. This disparity between model and field observations suggest microenvironments within bulk solutions may be important for greigite formation and retention. These constraints suggest greigite is more likely to form alongside pyrite in shallow, non-steady state aqueous solutions.

1. Introduction

Iron sulphide minerals are widely used as paleoclimatic indicators as their constituent iron and sulphur species are sensitive to environmental conditions (Roberts et al., 1996; Fu et al., 2008; Chen et al., 2021). Greigite (Fe_3S_4) is an iron sulphide that typically forms as an intermediate phase along the pyrite (FeS_2) reaction pathway (Berner, 1967; Hunger and Benning, 2007). As it is considered thermodynamically metastable with respect to pyrite, it was thought for a long time to be uncommon in natural environments (Machel and Burton, 1991; Roberts, 1995); however, it has been widely identified in shallow sediments due to its ferrimagnetic properties which contribute to palaeomagnetic readings (e.g., Snowball and Thompson, 1988; Rowan and Roberts, 2005, 2006). Greigite is thought to be preserved when pyritization, i. e., the transformation of precursor iron-sulphides to pyrite via sulphur addition, is arrested (Roberts and Turner, 1993; Wilkin and Barnes, 1997). This occurs either in sulphur-limited conditions, where low organic carbon content inhibits the presence of sulphate-reducing bacteria, or in the presence of abundant iron which use up reactive sulphur (Roberts and Weaver, 2005; Yang et al., 2022). The association of bacteria and balance between iron and sulphur means greigite has the potential to be a unique proxy for past environments, but only if its formation conditions are fully understood.

Greigite is frequently observed in low temperature, sulphidic sediments in continental marine (Kao et al., 2004; Liu et al., 2018), tidal (Keene et al., 2011; Burton et al., 2011) and inland lacustrine environments and wetlands (Wilkin and Ford, 2006; Nowaczyk, 2011). It forms in non-steady state, anoxic environments and is preserved due to alterations to geochemical conditions; this may be caused by tectonic subsidence altering sea levels and organic matter supply (Liu et al., 2018), large inputs of external iron-rich sediments (Kao et al., 2004), and possibly methane diffusion in submarine sediments (Rudmin et al., 2018). Variations in geochemical conditions may alter the dominant reactant available for greigite formation. Under standard-state conditions (25 °C, 1 bar, 1 M) greigite forms from mackinawite (FeS) in aqueous solutions with excess sulphur (Rickard and Luther, 2007).

* Corresponding author.
E-mail addresses: j.turney20@imperial.ac.uk (J.N. Turney), d.weiss@imperial.ac.uk (D. Weiss), adrian.muxworthy@imperial.ac.uk (A.R. Muxworthy), alastair.fraser@imperial.ac.uk (A. Fraser).

https://doi.org/10.1016/j.chemgeo.2023.121618
Received 20 January 2023; Received in revised form 21 June 2023; Accepted 28 June 2023
Available online 30 June 2023

There are several different reaction paths, for example: (1) Berner (1967) showed experimentally that greigite forms as an intermediate phase when mackinawite reacts with dissolved zerovalent sulphur (S^0) in the form of reactive sulphur species, (2) in acidic conditions, mackinawite partially dissolves to form Fe^{2+} and S^{2-}, which reacts with H^+ to produce H_2S, acting as the reactant to form greigite (Lin et al., 2018), and 3) in alkaline conditions, bisulfide (HS^-) and polysulfides (S_n^{2-}) act as a reactant instead of H_2S (Benning et al., 2000; Rickard and Luther, 2007). Polysulfides typically form during the dissolution of elemental sulphur by reactions with dissolved sulphide, or oxidation of H_2S or HS^- by ferric iron (Hartler et al., 1967; Hellige et al., 2012; Wan et al., 2014) and nitrate (Lin et al., 2009). At temperatures above 50 °C, the oxidation of mackinawite may form pyrrhotite ($Fe_{1-x}S$), providing an alternative to greigite as the intermediate phase along the pyrite reaction pathway (Sweeney and Kaplan, 1973; Aubourg et al., 2012).

The numerous reaction pathways along which greigite can precipitate make it difficult to fully understand the formation conditions of greigite using laboratory experiments only. In contrast, thermodynamic modelling allows the possibility to test the role of many parameters combined and in isolation, i.e., iron and sulphur concentrations, pH, redox potential (Eh), temperature, etc., and predict mineral assemblages that form under specific conditions (Brookins, 1988). Thermodynamic modelling is therefore a critical tool to simulate mineral precipitation in aqueous solutions and explore and identify reaction processes, fluid flow, and porosity and permeability changes (Steefel et al., 2015). While considering reactive transport is important in understanding processes in dynamic natural systems, a critical preliminary step is to gain a full understanding of the role master solution parameters such as pH, Eh, temperature, concentrations and elemental ratios play in mineral precipitation in the aqueous solution. This is achieved using thermodynamic reaction pathway modelling. Early thermodynamic pH-Eh diagrams for iron sulphides (e.g., Machel and Burton, 1991; Burton et al., 1993) did not include greigite as it was considered uncommon. Rickard, 2012b and Ning et al. (2014, 2015) included greigite to constrain its stability relative to mackinawite. Rickard, 2012b established that greigite formation is promoted in acidic solutions when iron concentrations are greater than sulphur. However, these studies omitted pyrite to observe precursor minerals, thus being representative of temporary states rather than conditions under which greigite may be preserved in the presence of end-member iron sulphides. A further limitation of these earlier thermodynamic models (Rickard and Luther, 2007; Rickard, 2012b) was missing thermodynamic greigite data in the literature, with Ning et al. (2015) using values from analogue iron sulphides. Only very recently the enthalpy for greigite has been experimentally determined by Subramani et al. (2020). This enabled Shumway et al. (2022) to demonstrate greigite may be thermodynamically stable relative to pyrite and pyrrhotite, at or below room temperature. This is supported by thermodynamic calculations by Son et al. (2022) which predicted greigite is more stable at the nanoscale in low-temperature alkaline and anoxic solutions. However, a critical constraint to understanding greigite precipitation in aqueous systems, is to identify the effect of elemental concentrations, i.e. Fe, S and pH, on different reaction pathways, at temperatures above 25 °C.

Here, we address this knowledge gap by studying the effect of iron and sulphur concentrations on greigite formation and preservation in aqueous solutions theoretically using the open source geochemical code PHREEQC. Firstly, we develop and test models that allow us to constrain reaction pathways in solutions with different chemical compositions (pH, Eh, Fe and S concentrations, Fe:S elemental ratios, temperature) and then identify conditions that promote or hinder the formation of greigite. Secondly, individual parameters, e.g., iron and sulphur ratios, are altered to identify the boundary conditions of greigite formation. Thirdly, model results are compared with observations in nature to provide further understanding of possible greigite forming environments.

2. Methods

Based on the work by Rickard, 2012b, we have developed reaction pathway models, using the PHREEQC computer program (Parkhurst and Appelo, 2013), to simulate greigite formation along multiple reaction pathways under different iron and sulphur ratios, pH and Eh, and temperatures above and below 25 °C. Pyrite and pyrrhotite have been included to constrain how greigite may form and be preserved in the presence of end-member iron sulphides. To identify the solution parameters required for greigite to be thermodynamically favourable relative to other iron sulphides, it was important to develop a database that included the minerals and thermodynamic properties for the different reaction pathways.

2.1. Database development

PHREEQC at present uses 13 databases containing minerals with associated reactions and thermodynamic properties. We first undertook a critical review of the pre-existing databases to identify the relevant minerals and reactions (Table S1). We used PHREEQC's minteq.dat database as the default database, as it contained most of the minerals of interest, however, there were some key omissions: (1) Pyrrhotite was added from the llnl.dat database (Table S1). (2) For the polysulfide pathway, the species S_6^{-2} was not present, and had to be back-calculated from other polysulfide species in the llnl.dat database (Table 1 & S1). (3) The nitrate models required the addition of $NO_2(g)$ and $N_2(g)$ to the minteq.dat database to be considered viable reactants (Table 1 & S2).

The thermodynamic properties for pyrite formation are well established (Robie, 1966; Lemire et al., 2020), however, values for mackinawite and greigite are limited. Of the 13 databases, four give an equilibrium constant (*logK*) of −45 for greigite and eight give a *logK* of −4.7 or − 3.6 for mackinawite when HS^- is the reactant (Table S1). The *logK* for mackinawite and greigite is calculated using the Gibbs free reaction energy, $\Delta_r G^0$ (Eq. 1):

$$\Delta_r G^0 = -2.303RTlogK \quad (1)$$

Where R is the gas constant (0.00199 kcal/mol.K) and T is temperature in kelvin. $\Delta_r G^0$ is the difference between the total Gibbs free energy of formation ($\Delta_f G^0$) of the products and the total $\Delta_f G^0$ of the reactants at standard temperature and pressure (Table S2). A first value published by Berner (1967) gives a $\Delta_f G^0$ for synthetic greigite of −69.4 kcal/mol (Table S2). Rickard and Luther (2007) and Lemire et al. (2020) calculated a $\Delta_f G^0$ for greigite of −73.7 kcal/mol and -73.9 kcal/mol, respectively. The reproducibility of similar values by these studies suggests the $\Delta_f G^0$ by Lemire et al. (2020) is reliable. We calculated a $\Delta_f G^0$ for mackinawite of −21.7 kcal/mol. This falls within the upper end of a 95% confidence interval based on previously reported experimental values ranging between −22.3 kcal/mol to −23.5 kcal/mol (Berner, 1967; Rickard, 2006; Lemire et al., 2020) (Table S2). A sensitivity analysis has been conducted comparing the *logK* used in this study with the Berner (1967) and original minteq.dat database values (Table S3) which showed minor differences. Although *logK* for reactions with H_2S have previously been calculated as 4.4 (Davison et al., 1999) and 3.1 (Benning et al., 2000) due to the variability in these values, Rickard and Luther (2007) noted that sulphide solubilities are typically presented using reactions with HS^-. Reactions with HS^- were tested as it was also the default reactant considered in the minteq.dat database (Table S1). Using thermodynamic properties from Lemire et al. (2020) and Grenthe et al. (1992), mackinawite and greigite have calculated *logK* values of −2.1 and −41.1 (Table S1), respectively. In comparison, the $\Delta_f G^0$ from Berner (1967) calculated *logK* values for mackinawite and greigite of −2.6 and −37.9, respectively. The original minteq.dat database produced lower *logK* values of −4.7 for mackinawite and − 45.0 for greigite, suggesting they are more insoluble. Comparing modelling results using these *logK* values show strong similarities, with initial greigite saturation

states varying by 6% to 7% (Table S3), suggesting our thermodynamic parameters are reliable.

To calculate *logK* for greigite and mackinawite at different temperatures, the reaction enthalpy, $\Delta_r H^0$, is used which is determined using formation enthalpy, $\Delta_f H^0$. Using $\Delta_r H^0$, PHREEQC automatically calculates *logK* using the van't Hoff equation (Eq. 2), provided *logK* at one temperature and the standard enthalpy at 25 °C are known:

$$logK_{T_2} - logK_{T_1} = \frac{\Delta_r H^0}{2.303R} \bullet \left(\frac{1}{T1} - \frac{1}{T2}\right) \quad (2)$$

where T_1 is the initial temperature and T_2 is the new temperature at which $logK_{T_2}$ is being calculated. No enthalpy values are provided in the databases for mackinawite or greigite. Previous work has produced values for troilite (FeS) of −24.2 kcal/mol which shares a similar chemical structure to mackinawite (Table S2) (Xu and Navrtosky, 2010; Subramani et al., 2020). Anderko and Shuler (1997) used values from Latimer (1952) to estimate a $\Delta_f H^0$ for mackinawite of −21.9 kcal/mol, suggesting the best accuracy can be obtained close to standard state conditions (Table S2). The $\Delta_f H^0$ for greigite was taken from Subramani et al. (2020). The low enthalpy value (−103.3 kcal/mol) suggests greigite is more likely to form in ambient temperatures. This is consistent with observations in natural environments as greigite is typically found in shallow sediments at lower temperatures (Otero et al., 2006; Fu et al., 2008), therefore, this value is considered reliable. For polysulfide species, values were taken from Kamyshny et al. (2007) (Table S2). Using these thermodynamic properties, $\Delta_r H^0$ and *logK* were then calculated for different reaction pathways (Table 1).

2.2. Reaction pathways for pyrite and greigite

Six different pyrite reaction pathways have been studied to compare which form greigite (Table 1). The thermodynamically stable reactant depends on pH and Eh of the aqueous solution (Rickard and Luther, 2007) (Fig. 1). H_2S is dominant in acidic, anoxic conditions, whereas HS^- is dominant in alkaline (pH ~7–8.6), anoxic conditions (Fig. 1a) (Brookins, 1988). In the literature, the most widely suggested reactant for the pyrite reaction pathway is S^0, comprising of elemental sulphur and polysulfides (Kamyshny et al., 2008). S^0 is stable in very acidic, oxic conditions (Fig. 1a). In anaerobic solutions, S^0 may dissolve to form polysulfides which become the dominant phase in very alkaline conditions (Fig. 1a) (Hunger and Benning, 2007). As S^0 is in a solid phase, an additional reaction is required (Table 1), where sulphur is in equilibrium with different aqueous species (Eq. 3–5).

$$\text{acidic (pH} <\sim 7) \quad \text{sulphur} + 2H^+ + 2e^- = H_2S \quad (3)$$

$$\text{alkaline (} \sim 7 < \text{pH} < 8.6) \quad \text{sulphur} + H^+ + 2e^- = HS^- \quad (4)$$

$$\text{highly alkaline (pH} > 8.6\text{)} \quad \text{sulphur} + 2e^- = S_2{}^- \quad (5)$$

As polysulfides are compounds part of the S^0 species (Kamyshny et al., 2008), the S^0 reaction pathway can be applied to the polysulfide model. Reactions with individual polysulfide species have also been tested using the most common natural species, such as S_5^{2-} (Table 1, S7) (Kamyshny et al., 2008). However, as these reactions only included a few of the possible polysulfide species, reactions with S^0 were preferred. The nitrate and iron-loss pathway have also been included as alternatives to sulphur species pathways (Fu et al., 2008; Blanchet et al., 2009).

2.3. Design of the reaction pathway models

We use thermodynamic reaction pathway modelling to examine the favourable iron sulphide minerals in different geochemical conditions and Fe:S concentrations. Our models predict the amount a mineral would precipitate in moles, under a given set of conditions, rather than calculate reactions that are ongoing. The first set of models use unbuffered aqueous solutions to represent a non-steady state solution where pH and Eh are free to change depending on the minerals that precipitate which subsequently alter iron and sulphur concentrations. Our initial solution consists of pure water with a specified pH and Eh (Fig. 2a). In order to assess the effect of iron and sulphur only, we decided against the introduction of other chemical constituents (organic and inorganic) as they complex with iron or sulphur effecting the ratio specified. As only iron and sulphur concentrations are added during the model experiments, the nitrate pathway requires nitrogen in the initial solution to provide a reactant for the experiment to run. To analyse the effect of varying amounts of reactive nitrogen in the solution, high and low concentration models have been conducted with 10^{-2} and 10^{-9} m of nitrogen, respectively. Minerals of interest are introduced subsequently to the reaction pathway model with their associated reactions. The pathway is selected based on the initial pH and Eh (Fig. 2a, Table 1).

Along the pyrite reaction pathway, the stoichiometric ratio of elements within the minerals becomes progressively sulphur-dominant from mackinawite (FeS) to pyrite (FeS_2). Kao et al. (2004) suggested greigite may be preserved in iron-rich environments which use up available sulphur and halt pyritization. It is important therefore to consider mineral precipitation in iron and sulphur-dominant solutions. To this end, a molar ratio of 3:1 was selected for iron (Fe/S) or sulphur-dominant (S/Fe) solutions (Fig. 2a). A molar ratio at 2:1 provides a good comparison, however, trends in the data are clearer at a higher ratio; as mineral precipitation is limited by the amount of the non-dominant element, increasing the ratio further produces negligible differences in results.

In our models, molality concentrations start at 10^{-12} m and were limited to a maximum of 10^{-2} m in 1 kg of water to match concentrations in nature (Brookins, 1988). After each concentration increment, we conducted ten iterations before moving to the next order of magnitude. As the model progressed, more iron and sulphur were added at that specified ratio, e.g., at S:Fe ratio of 3:1, the initial concentration is 3×10^{-12} m sulphur and 1×10^{-12} m iron, at the next increment this increased to 6×10^{-12} m iron and 2×10^{-12} m sulphur (Fig. 2b).

The minerals of interest for the equilibrium phase block and the saturation index (SI) were selected (Fig. 2a). As iron and sulphur are introduced to the model, the SI of a given mineral was calculated by the ion activity in solution (IAP) over the activity required for the mineral to be at equilibrium or a solubility product (K_{sp}). When SI = 0, $logIAP = logK_{sp}$ the solution is saturated with respect to the mineral. When $logIAP < logK_{sp}$ the solution is undersaturated with respect to the mineral, and when $logIAP > logK_{sp}$ the solution is supersaturated. Initially, minerals were set to a target SI = 0 to identify the favourable minerals under equilibrium; a mineral will dissolve or precipitate to attain the target SI. The target SI was then altered to promote mineral precipitation or dissolution in an undersaturated or supersaturated solution, respectively. For example, setting a target SI < 0 in the model setup means a mineral precipitates in solutions that are undersaturated with respect to that mineral, despite the reaction being thermodynamically unfavourable.

2.4. Approach to buffering the aqueous solutions with respect to pH and Eh

To test the effect of pH and Eh buffers, PHREEQC requires 'pseudo-phases' to be added to the phase block (Fig. 2a) (Eq. 6 and 7):

$$\text{pH\_fix H+} = \text{H} + log\_\text{k} = 0.0 \quad (6)$$

$$\text{pe\_fix e}- = \text{e} - log\_\text{k} = 0.0 \quad (7)$$

Within PHREEQC, pe was typically used before the program converts it in the graph setup to Eh using pe = Eh/59.2. Both pseudo-phases were manually added to the equilibrium phase block with the SI corresponding to the pH or Eh required. To buffer Eh, 10 mol of O_2 were added to the equilibrium phase block. To buffer pH, PHREEQC provides

Table 1
Compilation of the pyrite reaction pathways used in this study. Chemical reactions are given for each phase with their associated thermodynamic properties which have been calculated using data from Lemire et al. (2020). The enthalpy value for greigite reactions includes data taken by Subramani et al. (2020). The enthalpy has been converted from kilojoules to kilocalories to match units in the Minteq database. The tested conditions for each pathway have also been specified which have been selected based on a reactant's thermodynamic stability under specific conditions (Fig. 1). The full list of thermodynamic parameters used in this study, including comparisons with other studies (e.g., Robie and Hemingway, 1995), is provided in the supplementary material S1 and S2. Table S1 and S2 include a summary of thermodynamic parameters for pyrrhotite taken from Chase (1998), Chase et al. (1995) and Grønvold and Stølen, (1992).

Reactant	Tested conditions	Mineral	Reaction pathways	LogK	Enthalpy (kcal/mol)	References
H_2S	Acidic, anoxic pH 2 to 6 Eh −100 to −250 mV	Mackinawite Greigite Pyrite	$FeS + 2H^+ = Fe^{+2} + H_2S$ $Fe_3S_4 + H_2 = 3FeS + H_2S$ $3FeS_2 + 2H_2 = Fe_3S_4 + 2H_2S$	4.85 −1.633 −7.144	−8.9101 28.408 0.907783	Hunger and Benning (2007)
HS^-	Alkaline, anoxic pH 8 Eh −400 mV	Mackinawite Greigite Pyrite	$FeS + H^+ = Fe^{+2} + HS^-$ $Fe_3S_4 + 4H^+ = 2Fe^{+3} + Fe^{+2} + 4HS^-$ $FeS_2 + 2H^+ + 2e^- = Fe^{+2} + 2HS^-$	−2.13713 −41.1278 −18.479	−3.578 42.2473 11.3	Berner (1970) PHREEQC Minteq database
Zerovalent sulphur	Oxic, acidic pH 2 Eh +175 mV Sulphate/sulphide boundary	Sulphur Mackinawite Greigite Pyrite	$S + H^+ + 2e^- = HS^-$ $FeS + H^+ = Fe^{+2} + HS^-$ $Fe_3S_4 = 3FeS + S$ $3FeS_2 = Fe_3S_4 + 2S$	−2.11 −2.137 −6.476 −10.373	−4.2 −3.578 37.637 7.061	Berner (1970)
Polysulfide	Very alkaline, anoxic pH 10 Eh −550 mV	Sulphur Mackinawite Greigite Pyrite	$S + 2e^- = S^{-2}$ $FeS + H+ = Fe^{+2} + HS^-$ $Fe_3S_4 + S_5^{-2} = 3FeS + S_6^{-2}$ $3FeS_2 + S_3^{-2} = Fe_3S_4 + S_5^{-2}$	−15.026 −2.137 −6.721 −10.075	7.9 −3.578 38.521 7.3	Schoonen and Barnes (1991) Luther III, 1991Kamyshny et al. (2007)
Iron loss	Oxic to anoxic Alkali to acidic pH 6–8 Eh +150 to −150 mV	Mackinawite Greigite Pyrite	$FeS + H^+ = Fe^{+2} + HS^-$ $Fe_3S_4 + Fe^{+2} + H_2O = 4FeS + 0.5O_2 + 2H^+$ $FeS_2 + 0.5Fe^{+2} + 0.5H_2 = 0.5Fe_3S_4 + H^+$	−2.13713 −48.0203 −9.2972	−3.578 105.6595 0.6282	Wilkin and Barnes (1996)
Nitrite	Oxic to anoxic Alkali to acidic pH 6–8 Eh +180 to −60 mV	Mackinawite Greigite Pyrite N_2(g) NO_2(g)	$FeS + H^+ = Fe^{+2} + HS^-$ $Fe_3S_4 + 2NO_2 + Fe^{+2} + 2H_2O = 4FeS + 2NO_3^- + 4H^+$ $FeS_2 + 0.5Fe^{+2} + NO_2 + H_2O = 0.5Fe_3S_4 + NO_3^- + 2H^+$ $N_2 = N_2$ $NO_2 = 0.5\ N_2 + O_2$	−2.1371 −32.773 −22.442 −3.1864 8.9857	−3.578 59.257 11.5981 0 −7.91421	Fu et al. (2008) Blanchet et al. (2009)

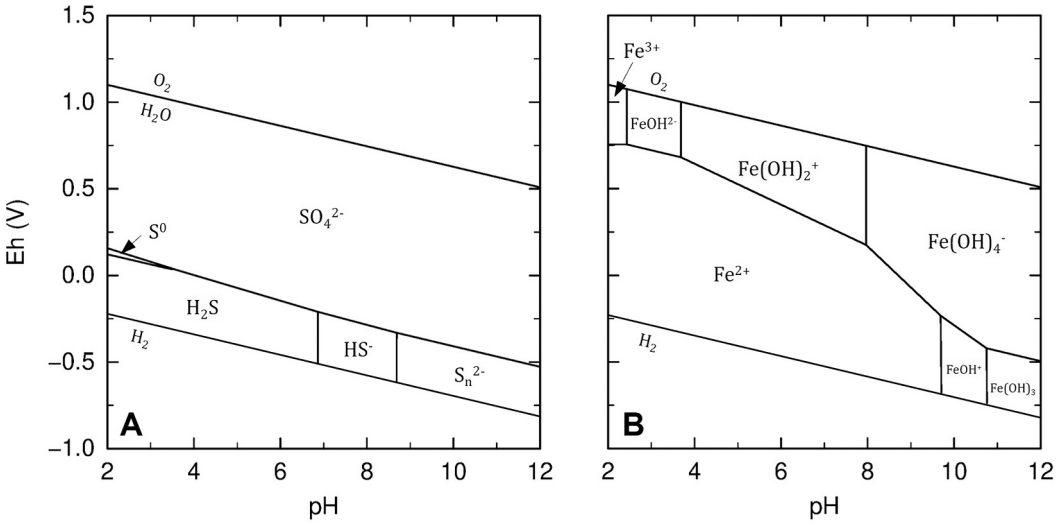

Fig. 1. Phase diagrams for the dominant iron and sulphur species at different conditions developed using PHREEQC. A shows the dominant sulphur species at an activity of 10^{-3} m and B shows dominant iron species at 10^{-6} m. Concentrations are representative of terrestrial waters (Brookins, 1988). Both phase diagrams are at standard state 25 °C at 1 bar pressure.

a numerical fix typically using a strong acid HCl, and sodium nitrate ($NaNO_3$). $NaNO_3$ is not a base or acid but is formed following neutralising a strong acid (HNO_3) and/or base (NaOH) and determines which one should be used to attain the required pH. If solutions become increasingly alkaline as the modelling experiment progresses, the donation of protons by HCl will maintain an acidic pH, whereas, to avoid solutions from becoming too acidic or to fix pH at an alkaline pH, NaOH produces OH^- to react with excess protons.

In our models, the complexation of Na^+ with sulphur species reduces the availability of reactive sulphur in the solution and lowers the SI of individual iron sulphide minerals. This means a minimum amount of $NaNO_3$ was added to the equilibrium phase block to reduce this effect. This technique works universally across the tested reaction pathways, providing the best opportunity to compare the likelihood of iron sulphide formation in different solution conditions.

3. Results

3.1. Iron sulphide precipitation in Eh and pH unbuffered aqueous solutions

In unbuffered modelling solutions, pH and Eh are altered by iron and sulphur concentrations and mineral precipitation. Fig. 3 shows iron sulphide precipitation as iron and sulphur are added to unbuffered solutions. As iron and sulphur are introduced, pH jumps to neutral irrespective of the initial conditions, whereas, Eh gradually changes as concentrations increase (Fig. 3). Iron-dominant solutions become increasingly anoxic and alkaline. The H_2S, HS^-, S^0 and iron-loss pathways favour pyrite at lower Fe/S ratios, and mackinawite in more iron-rich solutions (Figs. 3a, c & g). Conversely, sulphur-dominant solutions become acidic and Eh gradually increases, with only pyrite reaching saturation (Figs. 3b, d, f & h). The polysulfide pathway (Figs. 3c & d) is the exception as pyrite formation is less extensive in more anoxic and alkaline conditions. In the presence of polysulfides, mackinawite forms exclusively in iron-dominant solutions, whereas in sulphur-dominant solutions mackinawite is favourable at the lowest concentrations (Figs. 3c & d).

For the nitrate pathway, the point at which pyrite precipitates depends on the amount of nitrate present in the initial solution. At initial iron and sulphur concentrations of 10^{12} m, nitrate-rich solutions are less anoxic than nitrate-poor solutions, resulting in higher levels of undersaturation. In nitrite-rich solutions, pyrite precipitation occurs at higher iron and sulphur concentrations than nitrite-poor solutions. The drop in Fe/S ratio from above 10^7 to below 10^6 is caused by the injection of iron and sulphur at a higher order of magnitude, without an equivalent increase in sulphur removal by pyrite precipitation (Fig. 3e). Although mackinawite is not present, it is closer to saturation in nitrite-rich solutions due to less extensive pyrite precipitation.

Greigite is unstable in Eh and pH unbuffered solutions when minerals were set to a target SI = 0. The aqueous solutions remain undersaturated throughout, though greigite may be closer to saturation depending on the order of mineral precipitation and correlative changes in iron and sulphur concentrations.

3.2. Saturation index (SI) and molar iron to sulphur ratios

Figure 4 shows changes in SI depend on the initial conditions and on changes in iron and sulphur concentrations due to mineral precipitation. The more anoxic and alkaline the starting conditions, the less undersaturated solutions are with respect to all minerals. Sulphur species pathways show the most extensive mineral precipitation, whereas the iron-loss pathway show the most undersaturated SI (Table S9). For the nitrate pathway, nitrate-rich solutions are highly undersaturated at the lowest concentrations but at the point of mineral precipitation, solutions are less undersaturated than nitrate-poor solutions (Table S10).

Iron-dominant solutions are closer to saturation with respect to greigite than sulphur-dominant solutions (Figs. 4a & b). As iron and sulphur are introduced to the system, the aqueous solutions are less undersaturated with respect to greigite as they become progressively alkaline and anoxic (Figs. 4a). The partial removal of sulphur leads to heavily iron-rich solutions as pyrite precipitates (Fig. 4c). Solutions are less undersaturated with respect to greigite at these Fe:S concentrations (Fig. 4a) with an undersaturation index of six orders of magnitude for the H_2S, S^0, and nitrate pathways, and eight orders of magnitude for the HS^-. Mackinawite precipitation at higher Fe:S concentrations leads to a decrease in total sulphur (Figs. 4c & e). This correlates with more undersaturated solutions with respect to greigite (Fig. 4a).

Pyrite is strongly favoured in sulphur-dominant solutions. Iron removal from pyrite precipitation means solutions are undersaturated with respect to greigite (Figs. 4b, d & f). In regions of mackinawite precipitation, greigite is closer to saturation, with an undersaturation index of negative six in the polysulfide pathway (Figs. 4b & f).

While solutions remain undersaturated with respect to greigite, the concentrations at which pyrite and mackinawite precipitate influence

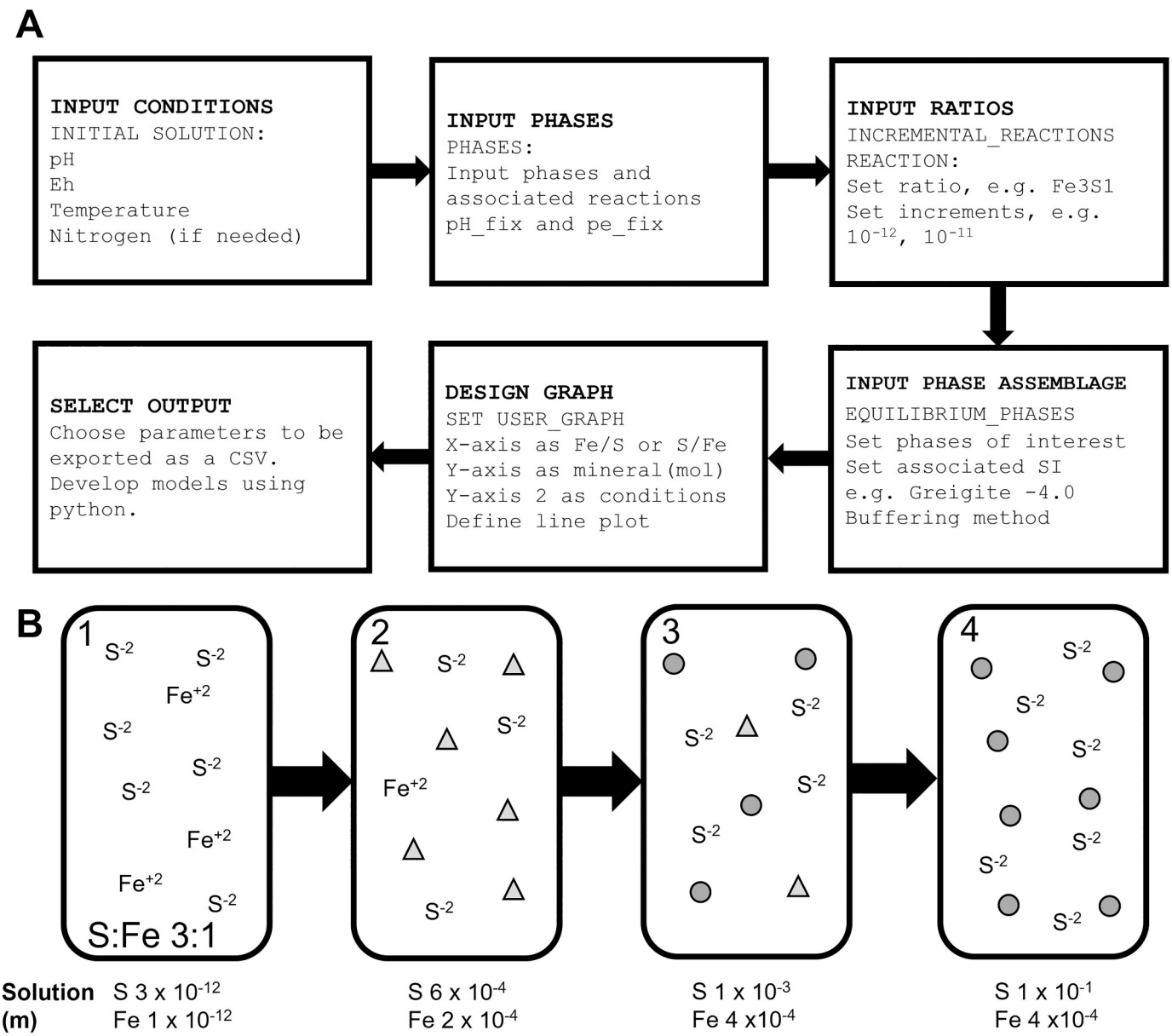

Fig. 2. Graphical representation of the reaction pathway model development. A is a breakdown of the model input. When the model is finalised, iron and sulphur start to be introduced into the solution at the initial conditions. B displays a schematic of the model as it progresses with 1) showing an input of sulphur and iron at a given ratio, 2) showing the point of initial mackinawite precipitation (triangle), 3) representing pyrite precipitation (circle) and alteration of the concentration ratio as it removes two parts sulphur to one part iron, and 4) demonstrating exclusive pyrite precipitation in heavily sulphur-dominant solutions, which is expected according to the sulphur-addition pathway.

the SI. Controlling the SIs within the equilibrium phase block can prevent or promote mineral precipitation and promote greigite formation within the models.

3.3. Altering saturation index (SI) to form greigite

There are two possible mechanisms to precipitate greigite in our models; (1) lowering the target greigite SI ($SI_{greigite}$) to enable precipitation when the solutions are undersaturated with respect to mackinawite and pyrite (Figs. 5a & d), and (2) lowering the $SI_{greigite}$ whilst increasing the target SI for pyrite (SI_{pyrite}) and/or mackinawite ($SI_{mackinawite}$) to limit their precipitation until a required level of supersaturation is reached (Figs. 5b & c). Lowering $SI_{greigite}$ controls what concentrations greigite starts to precipitate, whereas, increasing the target SI for other iron sulphides means greigite can form at higher concentrations.

In iron-dominant solutions, greigite precipitates in solutions when $SI_{greigite} = -7$ for the S^0, H_2S, and nitrate pathways (Fig. 5a). Greigite typically precipitates between pyrite and mackinawite, preventing mackinawite precipitation until higher Fe/S ratios (Fig. 5a). Alternatively, greigite precipitates in solutions when $SI_{greigite} > -7$ if $SI_{mackinawite} > 0$, preventing mackinawite precipitation until higher concentrations in more alkaline and anoxic conditions (e.g., Fig. 5c). For the S^0 and H_2S pathways, setting $SI_{mackinawite}$ to +2 and $SI_{greigite}$ to −4 is enough for greigite to precipitate. Extensive mackinawite formation in the presence of polysulfides means that for greigite formation, solutions must have a $SI_{mackinawite}$ greater than three (Fig. 5c). Mackinawite does not reach saturation in the nitrate pathway therefore, for greigite to precipitate a $SI_{greigite}$ of negative seven is required. In iron-dominant solutions, setting a SI_{pyrite} above zero to promote greigite formation is

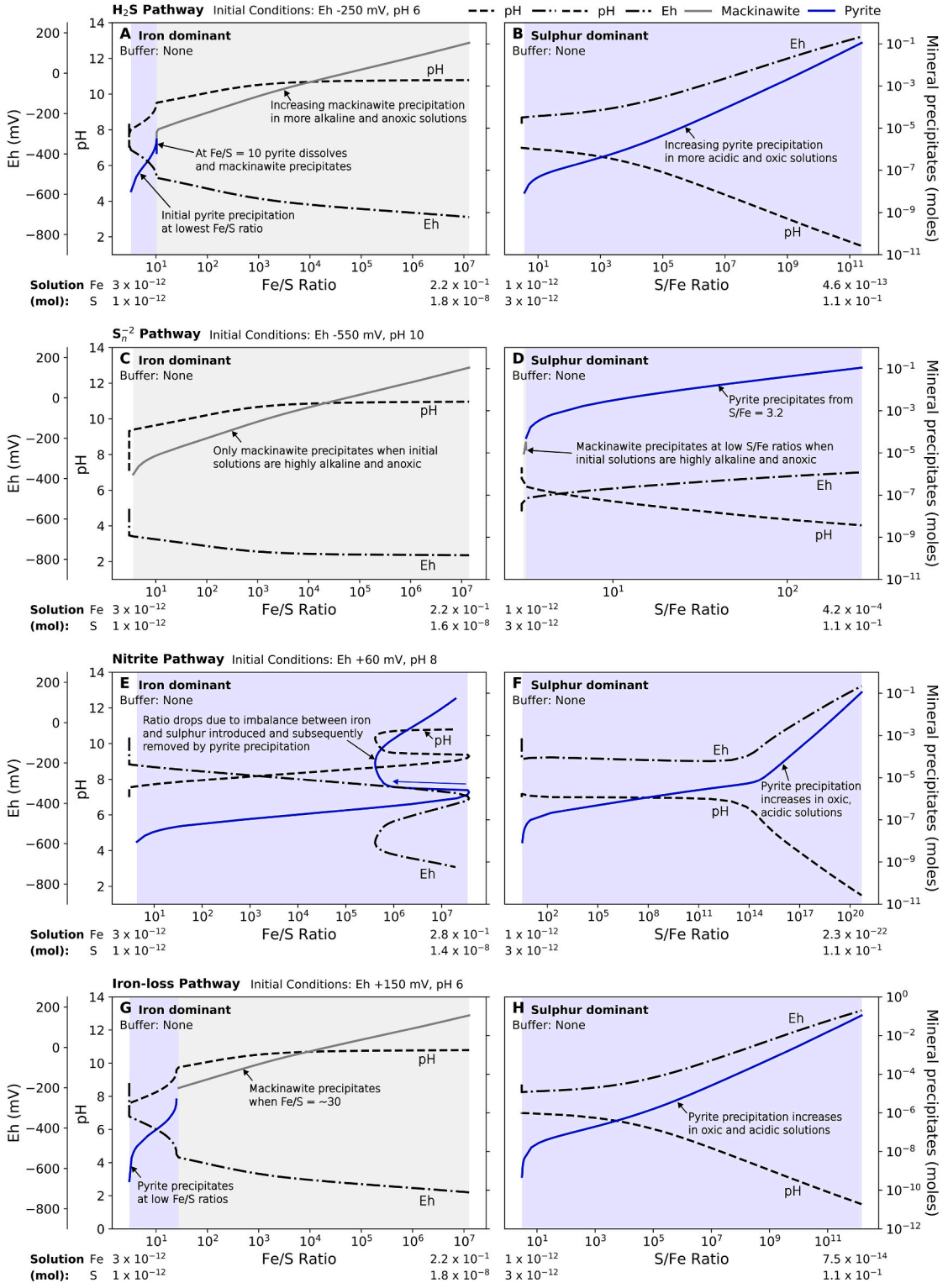

Fig. 3. Reaction pathways showing iron sulphide precipitation using different reactants under varying conditions and iron-sulphur ratios. Solutions are unbuffered and the SI for all minerals is zero. The left column shows iron-dominant solutions, and the right column is for sulphur-dominant solutions. Blue and grey shaded areas represent regions of pyrite and mackinawite precipitation, respectively. A and B represent iron sulphide precipitation for the H_2S pathway, with initial conditions being acidic and anoxic. C and D show precipitation from highly alkaline, anoxic initial conditions using polysulfides. E and F shows exclusively pyrite using nitrate, with solutions being oxic and alkaline initially before becoming anoxic at the start of the model. The blue arrow highlights a drop in Fe/S ratio when added iron and sulphur is increased by one order of magnitude, without a subsequent increase in sulphur removal by pyrite precipitation. G and H show the iron loss pathway, with solution conditions initially being set to very oxic and acidic, although shift to anoxic at the start of the model experiment. Except for the polysulfide pathway, in iron-dominant solutions, pyrite is preferred at the lowest Fe/S ratios and mackinawite precipitates in heavily iron-rich alkaline and anoxic solutions following sulphur removal via pyrite precipitation. Sulphur-dominant solutions show extensively pyrite in increasingly oxic, acidic conditions. The full list of results for the models is provided in the supplementary material S4-S12. (For interpretation of the references to colour in this figure legend, the reader is referred to the web version of this article.)

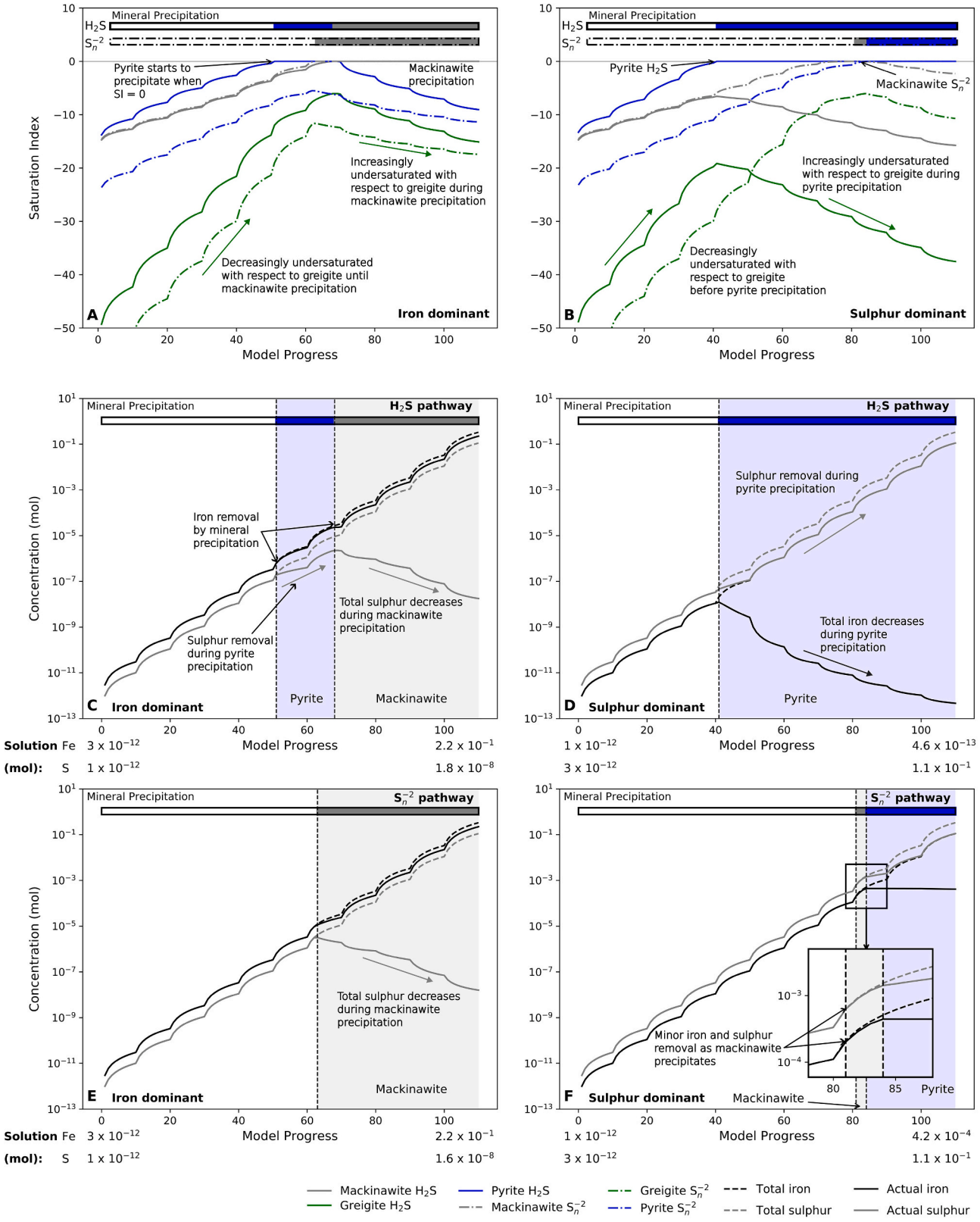

Fig. 4. Progression of saturation index and iron and sulphur concentrations along the reaction pathway for the H_2S and S_n^{2-} pathways using unbuffered solutions. The target SI for mineral precipitation for all minerals is zero. A and B represent changing SIs in iron and sulphur-dominant solutions, respectively, for the H_2S and S_n^{2-} pathways. C to F show changes in iron and sulphur concentrations as minerals reach saturation and precipitate for iron-dominant (c, e) and sulphur-dominant (d, f) solutions. Mineral precipitation is represented by shaded areas with grey for mackinawite, blue for pyrite and white for no precipitation. These pathways have been chosen as they highlight how SI is affected by mackinawite and pyrite precipitation in iron and sulphur-dominant solutions. Mackinawite and pyrite precipitation has similar effects on SI in all models. The full list of model pathway results, including for nitrate, iron-loss and other sulphur species are provided in the supplementary material S4-S12. (For interpretation of the references to colour in this figure legend, the reader is referred to the web version of this article.)

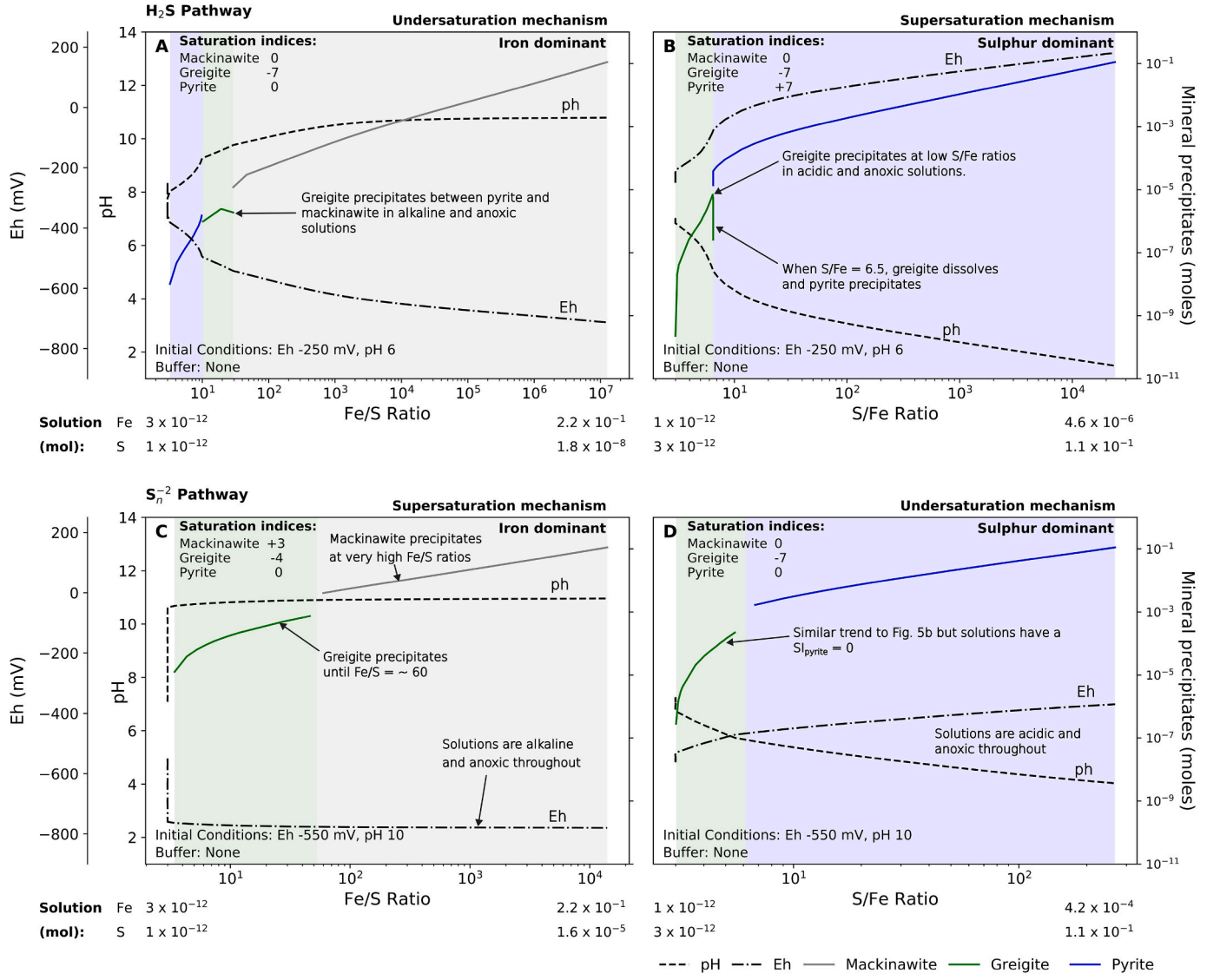

Fig. 5. Reaction pathways showing greigite precipitation by altering the target saturation indices under varying conditions using unbuffered solutions. The left column shows iron-dominant solutions, and the right column is for sulphur-dominant solutions. Green shaded areas represent regions of greigite precipitation, and grey and blue represent mackinawite and pyrite precipitation, respectively. A and D predict greigite precipitates when $SI_{greigite} = -7$ in iron and sulphur-dominant solutions for the H_2S and polysulfide pathways, respectively. B and C show greigite precipitation when solutions have a $SI_{greigite}$ below zero and a SI_{pyrite} and $SI_{mackinawite}$ above zero in the sulphur-dominant H_2S and iron-dominant polysulfide pathways, respectively. For B, the solution has a $SI_{greigite}$ of negative seven and a SI_{pyrite} of positive seven. C shows that greigite precipitates in solutions where $SI_{greigite} = -4$ and $SI_{mackinawite} = +3$. The small gap in precipitation between a ratio of 10 and 100 in C and below a ratio of 10 in D is a result of the model step size when introducing iron and sulphur. The full list of results for the altered SI models are provided in the supplementary material S12. (For interpretation of the references to colour in this figure legend, the reader is referred to the web version of this article.)

largely ineffective as pyrite forms at lower iron and sulphur concentrations than mackinawite and greigite.

In sulphur-dominant solutions, greigite precipitation requires a SI of greater than zero for pyrite and less than zero for greigite due to extensive pyrite precipitation when all minerals have a target SI = 0 (Fig. 5b). For the polysulfide pathway, greigite precipitates in solutions when $SI_{greigite} = -7$ (Fig. 5d), however, greigite can precipitate in solutions when $SI_{greigite} > -7$ provided $SI_{mackinawite}$ and $SI_{pyrite} \geq +1$. Although such conditions seem to improve greigite formation potential, supersaturating with respect to pyrite may allow other iron sulphides, such as pyrrhotite, to form in nature which can have adverse effects on greigite formation.

3.4. Effect of temperature change on greigite formation

The pH-Eh diagrams (Fig. 6) show how temperature changes affect the stability of iron sulphides. Pyrrhotite has been incorporated as it occurs widely in hydrothermal, igneous, and metamorphic systems (Roberts, 2015; Horng, 2018). In sulphur and iron-dominant reaction pathways, pyrrhotite replaces mackinawite directly leading to a different reaction path. Pyrrhotite is stoichiometrically similar to mackinawite so has the same effect on iron and sulphur concentrations as it precipitates (Table S4-S12). The stability of pyrrhotite means solutions are more undersaturated with respect to greigite than with pathways without pyrrhotite. Greigite precipitates in solutions at $SI_{greigite} = -9$ when $SI > 0$ with respect to other iron sulphides (Fig. 6).

At higher temperatures, solutions are more undersaturated with respect to all iron sulphide minerals. The SI for pyrrhotite is least

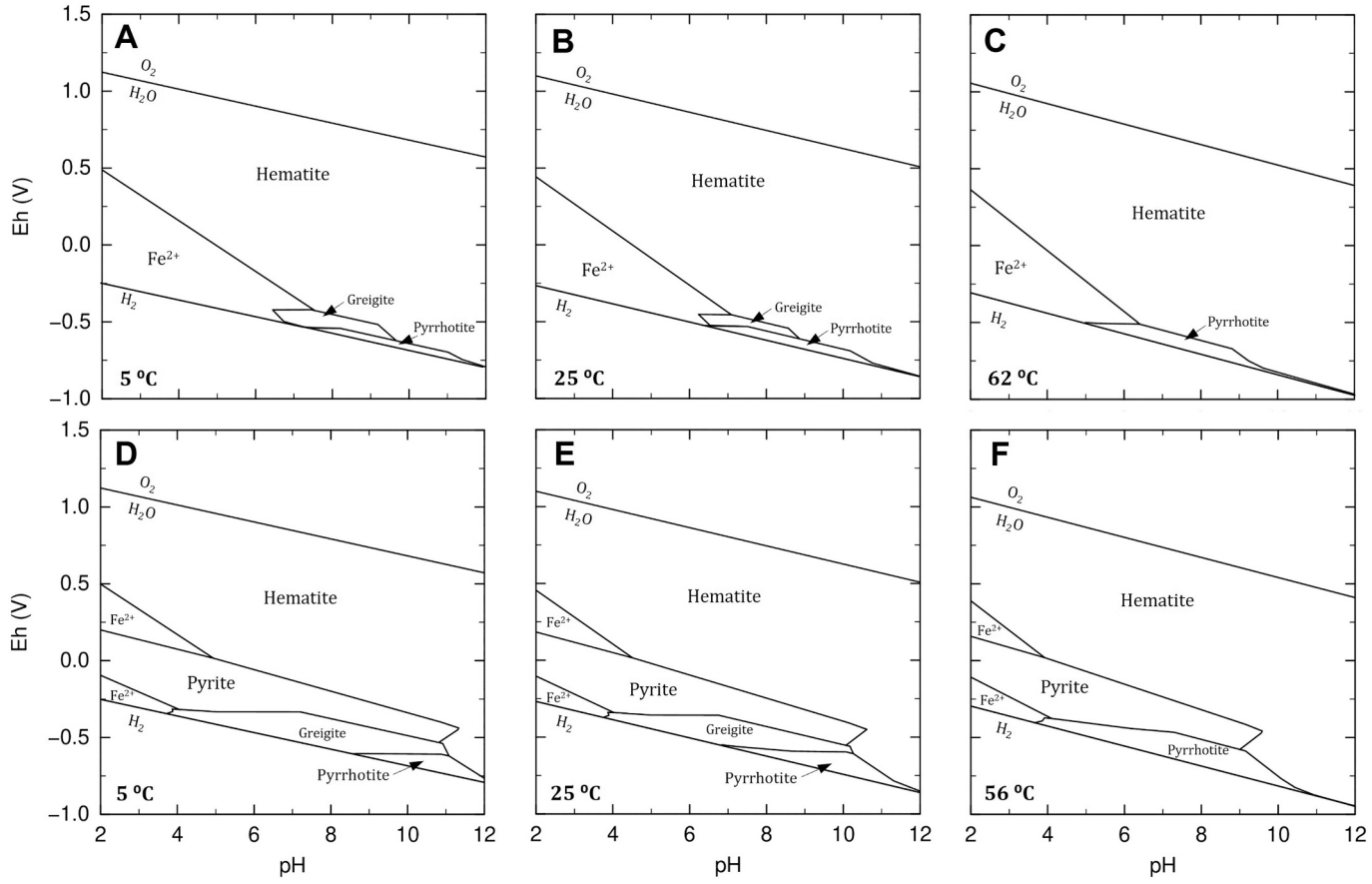

Fig. 6. Phase diagrams predicting greigite regions in iron-dominant (a-c) and sulphur-dominant (d-f) solutions at different temperatures. Iron-dominant solutions have target saturation states of −9 for greigite and + 1 for mackinawite and pyrrhotite, when iron is 1.5×10^{-2} m and sulphur is 1×10^{-2} m, and sulphur-dominant solutions have target saturation states of −9 for greigite and + 2 for pyrite when iron is 1×10^{-2} m and sulphur is 1.5×10^{-2} m. Hematite is included to represent ferric-iron bearing minerals found in oxic environments.

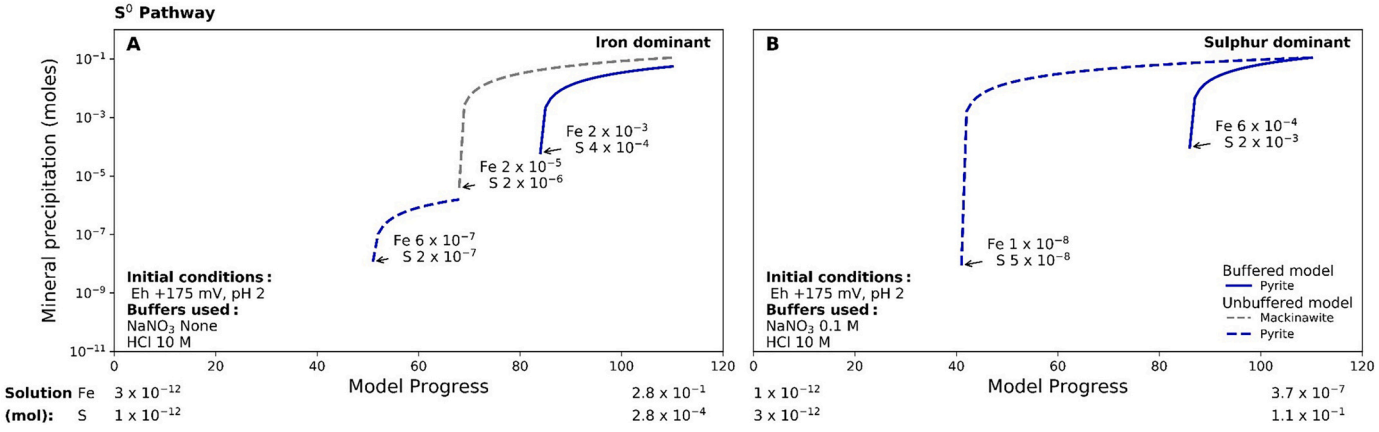

Fig. 7. S^0 reaction pathway under buffered conditions with Eh = +175 mV and pH = 2. Solutions are unbuffered and the target SI for all minerals is zero. A) is for the iron-dominant solution, comparing mineral precipitation between buffered and unbuffered solutions. The initiation of pyrite precipitation at higher concentrations of 2×10^{-3} m Fe and 4×10^{-4} m S means mackinawite is no longer present. B) compares pyrite precipitation in sulphur-dominant solutions. Pyrite formation occurs at significantly higher concentrations using buffered solutions when sulphur (2×10^{-3} m) is over half an order of magnitude greater than iron (6×10^{-4} m). The full list of buffered model results is provided in the supplementary material S4-S12.

effected and SI for greigite is most effected as temperatures increase. In iron and sulphur-dominant solutions where the target SI has been altered, greigite is closer to saturation at lower temperatures at and below 25 °C (Figs. 6a & d). For iron-dominant solutions, greigite is preferred in alkali, anoxic solutions between hematite and pyrrhotite. As temperatures increase, greigite becomes more unstable and is replaced by pyrrhotite (Fig. 6c). Extensive pyrite in sulphur-dominant solutions reduces the temperature range at which greigite is preferred (Figs. 6d-f). Below 25 °C greigite is preferred from highly acidic to alkali, anoxic conditions (Fig. 6d). Lowering the $SI_{greigite}$ increases the temperature range at which greigite is preferred. For example, greigite is preferred up to 62 °C when $SI_{greigite} = -9$ and up to 95 °C when $SI_{greigite} = -10$ in

iron-dominant solutions. Furthermore, greigite is closer to saturation as temperatures decrease. At 5 °C, greigite precipitates in solutions when $SI_{greigite} = -6$, compared to −9 at 25 °C. These temperature observations are in line with observations of greigite in shallow sediments (e.g., Kuwabara et al., 1999; Otero et al., 2006), provided solutions are unbuffered.

3.5. Iron sulphide precipitation in pH and Eh buffered solutions

Figure 7 shows pH and Eh buffered solutions have similar SI trends to unbuffered solutions, but the extent of mineral formation is generally less. Oxic conditions have strongly adverse effects on mineral formation. In acidic, oxic solutions, the S^0, nitrate and iron-loss pathways show pyrite is favourable at comparatively higher concentrations than unbuffered solutions (Fig. 7). No mineral precipitation occurs in alkaline solutions for the nitrate and iron-loss pathways (Table S9 & S10). In iron-dominant solutions, mackinawite is generally absent (Fig. 7a). The exception is the polysulfide buffered solution, where mackinawite is favourable when iron is an order of magnitude greater than sulphur. Generally, mineral precipitation using buffered solutions is less extensive and may initiate at concentrations a few orders of magnitude higher (Fig. 7).

Buffered solutions are more undersaturated with respect to greigite than unbuffered solutions. The exceptions are the polysulfide and HS^- pathways where solutions are alkaline and anoxic. In sulphur-dominant buffered solutions, greigite is closest to saturation when polysulfides are the reactant. Before mackinawite precipitation, greigite reaches the same level of undersaturation as the unbuffered solutions. Greigite precipitates at the lowest S/Fe ratios in the polysulfide pathway when solutions have a $SI_{greigite}$ of negative seven. Greigite precipitates between pyrite and mackinawite when the solution has a $SI_{mackinawite}$ greater than zero. Except in the presence of polysulfides, solutions are more undersaturated with respect to greigite than unbuffered solutions, although anoxic, alkaline conditions universally reduce the extent of undersaturation.

4. Discussion

Our reaction pathway modelling predicts that greigite is closer to saturation in low-temperature anoxic and alkaline solutions. This is supported by similar thermodynamic predictions by Shumway et al. (2022) and Son et al. (2022). Our modelling predicts greigite precipitates in solutions when $SI_{greigite} < 0$. Solutions are closer to saturation with respect to greigite when SI > 0 with respect to other iron sulphides (Fig. 6). When all minerals are at equilibrium, greigite typically reaches closest to saturation in iron-dominant solutions with minor sulphur input (Figs. 4 & 5).

4.1. Identification of boundary conditions for greigite formation and stability in aqueous solutions

Our modelling results show Eh and pH are master variables controlling greigite precipitation. Iron-dominant unbuffered solutions show precipitation occurs in progressively alkaline and anoxic conditions, from pyrite to greigite to mackinawite (Figs. 5a & c). As unbuffered sulphur-dominant solutions become more acidic and oxic at higher S/Fe ratios, greigite is closer to saturation at the lowest S/Fe ratios (Figs. 5b & d). Sulphur-dominant solutions are substantially undersaturated with respect to greigite unless pH and Eh are buffered in alkaline and anoxic conditions, with polysulfides as possible reactants (Fig. 4). Unbuffered and buffered solutions show similar trends, with precursor iron sulphide precipitation becoming more extensive in anoxic conditions, and pyrite being favoured as Eh increases (Fig. 7).

4.1.1. The role of Eh and pH

Reaction pathway modelling shows solutions are closer to saturation with respect to greigite in anoxic conditions with Eh at and below −500 mV for all sulphur species pathways (Figs. 5 & 8). Although the S^0 pathway precipitates pyrite at +175 mV at a highly acidic pH (Fig. 7), at a pH typically associated in greigite-hosted sediments, mineral formation is not extensive until Eh is lowered to more than −150 mV. For alternative

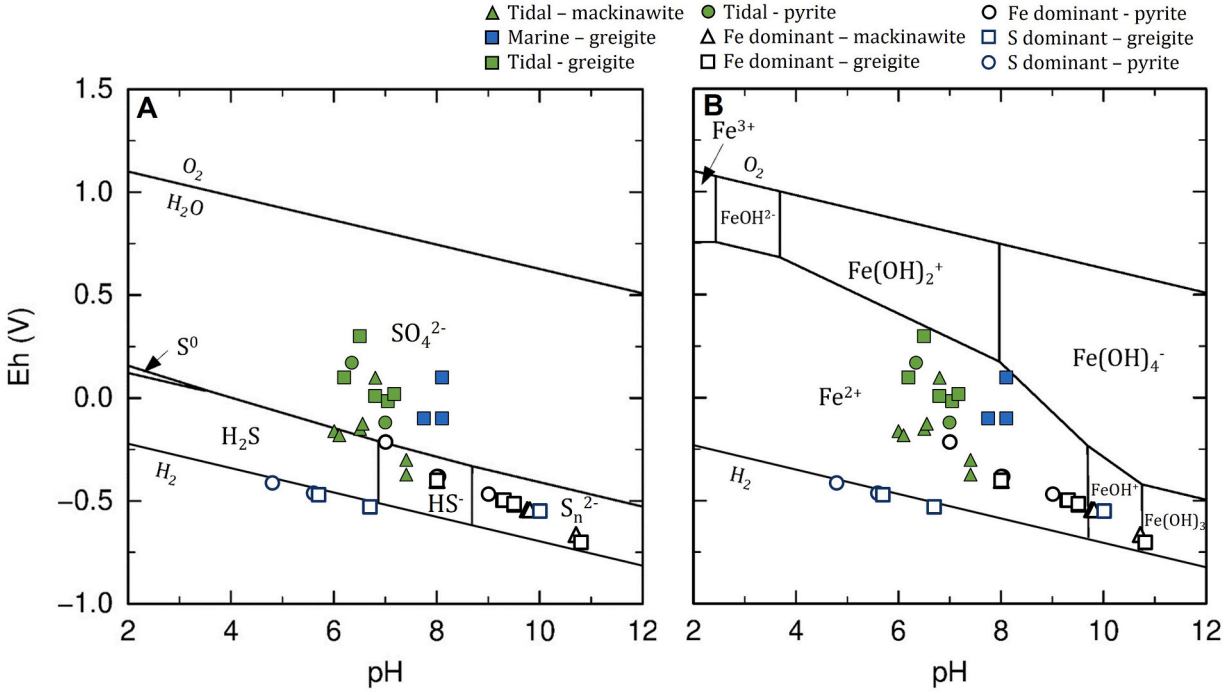

Fig. 8. Eh-pH diagrams for iron and sulphur containing phases comparing iron sulphide-hosted sediments with solution conditions at the point of precipitation in the models. Models chosen required the least alteration to SI for greigite to form. The full list of data is provided in the supplementary material S13-S14. Data is taken from Burton et al. (2006a, 2006b, 2011), Fu et al. (2008), Gao et al. (2009), Kao et al. (2004), Keene et al. (2011), Otero et al. (2006). Pyrrhotite is not included as it was not observed in the geochemical studies, therefore, the models without pyrrhotite provide a better comparison and more accurately depict shallow, low-temperature aqueous environments.

pathways, the iron-loss and nitrate pathways show precipitation is more common in acidic conditions, but solutions remain heavily undersaturated with respect to all iron sulphides unless conditions are buffered at a lower Eh. Nitrate and iron-loss are oxidation pathways, therefore, the high levels of undersaturation in oxic conditions may be due to the models representing a dissolution-reprecipitation pathway. Furthermore, as models focus on the relationship between iron and sulphur, the nitrate pathway is dependent on the amount of nitrate input from either the initial solution or provided by $NaNO_3$ in buffered solutions. Although the diffusion of oxygen or nitrate into shallow sediments has been suggested to form greigite (Fu et al., 2008; Blanchet et al., 2009), our modelling results suggest that in systems where iron and sulphur are available, sulphur species will be thermodynamically favoured to nitrate and iron-loss pathways. As model conditions become more anoxic, the higher availability of reactive Fe^{2+} and S^{2-} aids greigite formation and potential preservation, whereas the speciation and source of ions is largely dependent on the pH.

Using pH-Eh diagrams, Rickard (2012b) argues that greigite forms in favour of mackinawite in acidic, oxic conditions. However, the introduction of pyrite in our models highlights greigite is closer to saturation in the presence of pyrite in alkaline conditions. Greigite precipitates in acidic sulphur-dominant solutions (Fig. 5b), but this requires more significant alterations to saturation states than alkaline, iron-dominant solutions (Fig. 5a). Greigite typically forms above a pH of 8, with mackinawite being favoured in more extreme alkaline conditions (Figs. 3, 5 & 8). As mackinawite forms readily in sediments, its solubility is a vital control for iron and sulphur concentrations and the potential for greigite to form along the pyrite reaction pathway (Gregory et al., 2014; Rickard, 2019). At low temperatures, mackinawite dissolves in acidic conditions and forms greigite, but the availability of iron and sulphur increases the rate of pyrite precipitation (Rickard, 2006), whereas, in very alkaline conditions, mackinawite and greigite becomes far less soluble, slowing the rate of pyrite formation (Schoonen and Barnes, 1991; Benning et al., 2000). Our results suggest pyrite is favoured in acidic conditions (Fig. 3d) and greigite is unlikely to be preserved. Mackinawite precipitation in very alkaline conditions (Figs. 3, 5, & 8) may mean that greigite formation requires a temporary drop in pH, but for greigite retention, pH needs to increase to arrest the dissolution-reprecipitation pathway to pyrite. Alternatively, the insolubility of mackinawite in very alkaline conditions means that the source of iron and sulphur for greigite formation may be pH independent (Schoonen and Barnes, 1991; Rickard, 2019). For the preservation of greigite, Duverger et al. (2020) and Berg et al. (2020) suggested ferric iron-bearing minerals, such as goethite, may provide a source for iron when subjected to reducing conditions, whilst bacteria may provide a source for polysulfides.

4.1.2. The role of pyrrhotite and temperature

Solutions are more undersaturated with respect to greigite when pyrrhotite is incorporated into the models. Our modelling predicts pyrrhotite is thermodynamically favourable at temperatures above 25 °C as solutions become more undersaturated with respect to other iron sulphides (Fig. 6).

Pyrrhotite rather than greigite is often observed in anoxic conditions (Kao et al., 2004) and at greater burial depths where temperatures are elevated (Aubourg et al., 2012). Wilkin and Barnes (1997) suggested at higher temperatures greigite formation is less common due to rapid pyrite nucleation. Previous studies have shown synthesized greigite can persist at temperatures of 100 °C in the presence of polysulfides (Wada, 1977) and 200 °C as a precursor to pyrite framboids (Wilkin and Barnes, 1997). Additionally, White et al. (2015) and Gorlas et al. (2018) identified greigite within submarine hydrothermal vents towards 100 °C via abiotic and biotic mechanisms, respectively. Rudmin et al. (2019) suggested a mixture of iron-rich brine and hydrothermal fluids precipitated accessory greigite with pyrrhotite in marine sediments. Our modelling results suggest for greigite to precipitate at higher temperatures requires more significant alterations to SI. Conversely, in low-temperature environments, Lennie et al. (1995) and Roberts (2015) showed that mackinawite to pyrrhotite transformation is very slow, allowing for the conversion to greigite. As kinetics have not been incorporated in this study, our models may represent shallow low-temperature environments where pyrrhotite is omitted and greigite is more likely to be the intermediate phase.

Our results affirm that greigite formation potential improves at and below 25 °C (Shumway et al., 2022; Son et al., 2022) (Fig. 6). Greigite precipitates closer to saturation in solutions below 25 °C. In addition, our modelling predicts that by altering the SI, greigite can precipitate across a greater temperature range. These results provide further constraints for the formation and retention of greigite in shallow sediments, with greigite-hosted sediments in marine settings recording temperatures of approximately 6 °C, ranging up to 15 °C (Kuwabara et al., 1999; Fu et al., 2008) (Table S14).

4.1.3. The role of saturation states (SI)

Our modelling results predict greigite precipitates in solutions when $SI_{greigite} < 0$ and $SI_{mackinawite}$ and $SI_{pyrite} \geq 0$ (Fig. 5). In iron-dominant solutions, a $SI_{greigite}$ of negative seven leads to greigite precipitation between pyrite and mackinawite (Fig. 5a). Sulphur-dominant solutions are heavily undersaturated with respect to greigite, therefore greigite precipitation and retention is aided by increasing the $SI_{mackinawite}$ and SI_{pyrite} by at least one or two orders of magnitude (Fig. 5b). The exception is the polysulfide pathway as greigite is closer to saturation due to the precipitation of mackinawite and precipitates in solutions where $SI_{greigite} = -7$ and $SI_{mackinawite}$ and $SI_{pyrite} = 0$ (Fig. 5d).

In undersaturated freshwater and marine environments, iron sulphide minerals can precipitate around organic surfaces (Helz, 2014; LaFond-Hudson et al., 2018). The reduction of millimolar sulphate and iron hydroxides adjacent to the surface produces large degrees of supersaturation from sulphide and Fe^{2+} despite bulk solutions being undersaturated (LaFond-Hudson et al., 2018). Our modelling results predict that greigite precipitates in iron-dominant solutions when $SI_{greigite} = -7$, therefore, for greigite to precipitate the adjacent solution would have to be more than seven orders of magnitude greater than the bulk solution. Similar observations have been made in undersaturated marine environments for minerals such as barite and halite, where solutions in microenvironments are supersaturated by up to eight orders of magnitude (Silva-Castro et al., 2013; Deng et al., 2019).

Model greigite precipitates closer to saturation when SI_{pyrite} and $SI_{mackinawite} > 0$. Supersaturating iron-dominant solutions with respect to mackinawite (Fig. 5c) is an unlikely mechanism as mackinawite typically forms readily in sediments (Rickard and Luther, 2007; Liu et al., 2017; Rickard, 2019). Conversely, in sulphur-dominant solutions greigite precipitates at greater Fe:S concentrations to mackinawite and lower Fe:S concentrations to pyrite, therefore, greigite precipitation requires a solution with a SI_{pyrite} greater than zero. Natural sulphide waters are typically supersaturated with respect to pyrite and either saturated or undersaturated with respect to precursor minerals (Schoonen and Barnes, 1991; Wilkin and Barnes, 1997; Li et al., 2011). This is due to pyrite nucleation being slow relative to iron sulphide precursors (Rickard, 2019), which has led to the formation of precursor iron sulphides in lake sediments. For example, Censi et al. (2017) and Marnette et al. (1993) calculated a supersaturation with respect to pyrite by seven and ~ 15 orders of magnitude, respectively, with the latter being undersaturated with respect to mackinawite and greigite by a few orders of magnitude. Our modelling predicts greigite formation requires far less significant supersaturation states. By increasing the SI with respect to pyrite, greigite can precipitate closer to saturation by several orders of magnitude.

4.2. The role of pH and Eh buffering

Unbuffered solutions show extensive mineral precipitation as Eh and pH are free to change depending on the iron sulphide that forms (Figs. 3 & 5). In comparison, buffered solutions only show extensive mineral

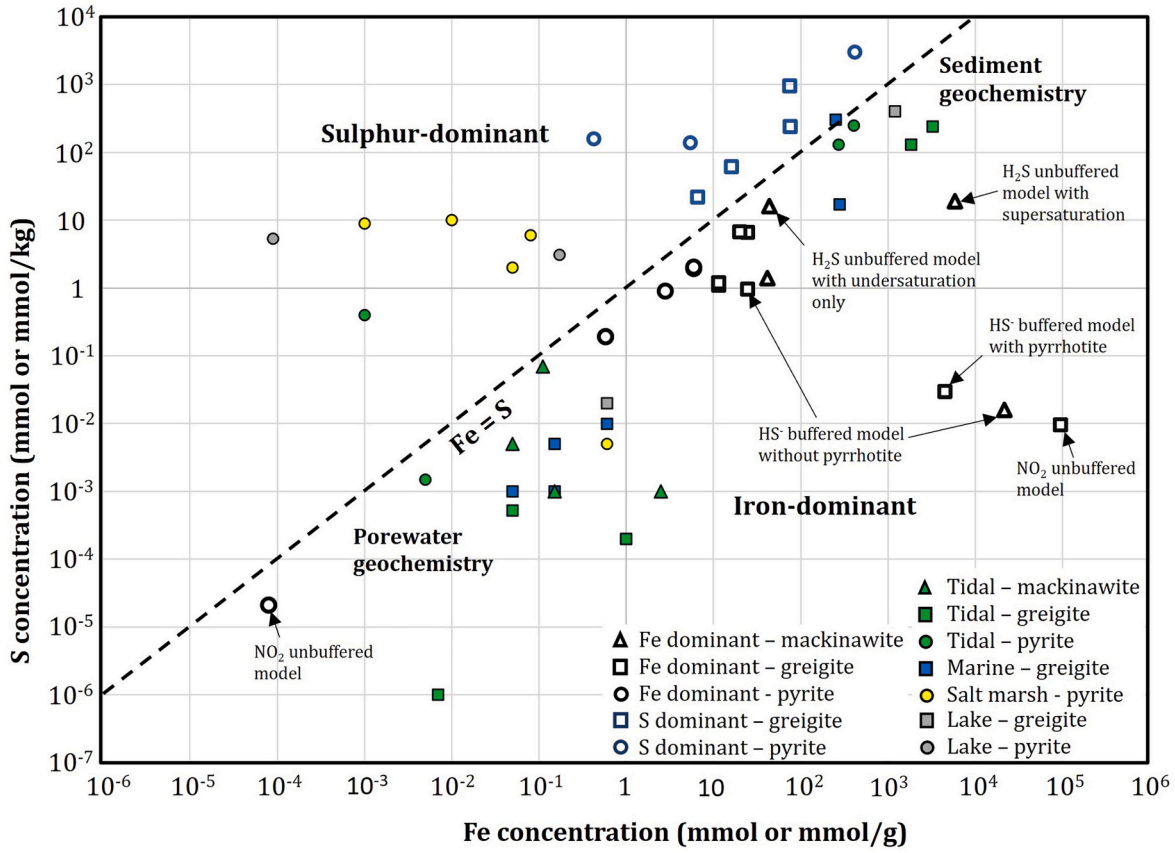

Fig. 9. Iron vs sulphur concentrations (millimolar) for iron sulphide-hosted sediments and for model results. An Fe=S line defines equal concentrations of iron and sulphur and divides greigite and pyrite zones which are typically iron and sulphur-dominant, respectively. The points at which mineral precipitation occurs along the reaction pathways is over an order of magnitude greater than natural sediments. Large disparities in iron and sulphur concentrations have been labelled. The full list of data is provided in the supplementary material S13-S14. Concentrations were taken from the literature either from the text, raw data or estimated from the figures (Aller, 1977; Perry and Pedersen, 1993; Bazylinski et al., 1995; Kostka and Luther III, 1995; Kuwabara et al., 1999; Koretsky et al., 2005; Burton et al., 2006a, 2006b; Otero et al., 2006; Gao et al., 2009; Burton et al., 2011; Holmkvist et al., 2011a, 2011b, 2014; Keene et al., 2011; Wong et al., 2013).

formation in alkaline and anoxic conditions, with greigite being closer to saturation in the HS^- and polysulfide pathways (Table S5 & S8).

The pH at which greigite precipitates in the iron-dominant HS^- pathway is similar to the buffered alkaline pH identified in greigite-hosted marine sediments, however, our modelling results show iron-sulphides typically precipitate at a lower Eh (Fig. 8). In marine environments, HS^- has been proposed as a viable reactant for greigite formation but only in non-steady state systems where terrigenous input alters the geochemical conditions and arrests pyritization (Fu et al., 2008; Blanchet et al., 2009). Although modern oceans are pervasively oxic, the redox chemistry can change from small external inputs of iron and sulphur, which may form reduced iron sulphide minerals (van De Velde et al., 2020). Our modelling results show iron-dominant unbuffered solutions become increasingly anoxic and alkaline as the elemental concentration becomes more iron-rich. If the pH remains buffered, our modelling results predict HS^- may be the favourable reactant to form greigite provided Eh is lowered, which can be caused by high sedimentation rates in marine settings.

In iron-dominant solutions, the role of buffers is represented by either HNO_3^- or HCl which add protons, preventing solutions from becoming too alkaline. The influence of buffers on greigite formation is not well established. In marine environments, humic acid may prevent pyrite nucleation as it dissolves iron-bearing minerals which then complex with organic matter (OM) (Morse and Wang, 1997). Additionally, Rickard et al. (2001) showed that in presence of the organic compound, aldehyde, the pathway of mackinawite dissolution and reprecipitation to pyrite is altered to a solid-state transformation to greigite. Our modelling results suggest that buffers may promote greigite formation in alkaline, anoxic solutions, whereas, using unbuffered solutions, greigite can form across a wider range of pathways from different initial conditions.

4.3. *Comparison of modelling results with natural systems regarding greigite formation and preservation*

Our modelling results show precursors mackinawite and greigite precipitate within the polysulfide region, whereas natural systems typically plot within sulphate and HS^- regions (Fig. 8a). Although most natural systems plot within the Fe^{2+} region, the precipitation of model greigite within the iron-hydroxide region suggest Fe(III)-bearing minerals may be a source of iron (Fig. 8b). In solutions where iron is abundant, pathway modelling and natural solutions show greigite is more likely to reach saturation (Fig. 9). However, higher concentrations and more extreme conditions observed in the models, may suggest greigite formation is aided by microenvironments rather than bulk waters.

4.3.1. *Porewater pH and Eh of iron sulphide-hosted sediments*

Model greigite precipitation within the alkaline, anoxic polysulfide region suggests polysulfides are viable reactants for greigite formation in solutions where $SI_{greigite} < 0$ (Fig. 8a). Extensive mackinawite precipitation suggests the polysulfide pathway is more likely to form greigite in iron-dominant solutions (Fig. 3c). In sulphur-dominant solutions, greigite and pyrite precipitation occurs outside the water stability zone (Fig. 8a). This implies polysulfides are unlikely to be stable as solutions become

increasingly sulphur-rich and acidic. As they are unstable and highly sensitive to oxidation, the understanding of polysulfide distribution in natural environments is limited (Rickard and Morse, 2005). Polysulfide data is rare for marine environments (Neretin et al., 2004; Holmkvist et al., 2014). In these studies, small amounts of polysulfides formed through reactions of free sulphide and excess elemental sulphur in solid phase, with the latter being present in abundance within greigite-rich layers. As equilibrium concentrations of polysulfides are considered relatively low compared to elemental sulphur, in areas of abundant dissolved sulphide, polysulfides are less likely to be the main pathway for pyrite formation. The low concentration of polysulfides in nature suggests greigite is more likely to form via the polysulfide pathway in sulphur-limited solutions (Hunger and Benning, 2007). Pathway modelling predicts that in alkaline solutions, polysulfides are the favourable reactant for greigite formation if solutions are iron-dominant.

The availability of ferrous iron is central to iron sulphide formation, where abundant Fe^{2+} and low sulphur arrests pyritization and improves the preservation potential for greigite (Kao et al., 2004; Rickard and Morse, 2005). The more extreme conditions seen in the H_2S and S^0 iron-dominant, and polysulfide sulphur-dominant unbuffered solutions, predict greigite and mackinawite precipitation close to and within the iron hydroxide region, respectively (Fig. 8b). Additionally, pyrite precipitation from very low concentrations in the nitrate pathway produces iron-enriched solutions (Figs. 3e & 9), where mackinawite and greigite precipitate at the iron hydroxide/oxyhydroxide boundary (Fig. 8b). In dynamic freshwater and marine environments, Fe(III)-bearing minerals have been proposed as a source of iron which can arrest pyritization (Holmkvist et al., 2011b; Yang et al., 2022). Cyclical periods of oxidation and reduction leads to their formation and dissolution, respectively, causing large enrichments in Fe^{2+} which use up available sulphur (Keene et al., 2011). At the surface of iron hydroxide minerals, ferric iron may oxidise sulphide to form polysulfides and elemental sulphur, which can react to produce iron sulphides (Wan et al., 2014). The precipitation of greigite in anoxic, alkaline solutions suggests greigite formation and preservation is thermodynamically preferred in conditions where polysulfides and iron hydroxides are stable reactants.

4.3.2. *Porewater concentrations of iron sulphide-hosted sediments*

Figure 9 compares iron and sulphur concentrations from iron sulphide-hosted sediments and model data. Porewater and modelling predictions show similar disparities in iron and sulphur concentrations for iron sulphide precipitation. Pyrite preferentially precipitates when sulphur is an order of magnitude greater than iron, whereas greigite forms when iron and sulphur differ by over one order of magnitude (Figs. 5a, 9). Greigite can reach close to saturation in sulphur-dominant model solutions when sulphur and iron concentrations are within the same order of magnitude (Fig. 9). Literature porewater data for mackinawite is sparser due its rapid formation and short life span (Rickard, 2012a, 2012b). Modelling predictions and natural geochemical observations highlight mackinawite forms in iron-rich solutions when iron is typically greater than sulphur by more than one order of magnitude (Fig. 9). Despite these similarities, iron and sulphur concentrations required for mineral formation in our models typically lie two or more orders of magnitude greater than bulk porewater, and one to two orders less than sediment concentrations (Fig. 9). This implies that the models may be representative of concentration enrichments within microenvironments rather than bulk waters.

Microenvironment and bulk water conditions are heterogenous, therefore, minerals can precipitate that are considered thermodynamically unfavourable. The association of microorganisms and greigite has been identified in the vicinity of sulphate-reducing bacteria (SRB) (Gramp et al., 2010; Gorlas et al., 2018; Picard et al., 2018). Bacteria have a negative surface charge that attract cations in the solution and cause steep increases in concentrations adjacent to the cell walls (Ferris et al., 1988; Schultze-Lam et al., 1996; Hoffmann et al., 2021). Cation absorption by microorganisms has been identified to form precursor iron sulphides, by Duverger et al. (2020), at similar millimolar iron concentrations identified in our models. Model greigite precipitation in iron-rich aqueous solutions with minor sulphur input may indicate SRB enhance the potential for greigite formation and retention, if S^{2-} production is limited relative to Fe^{2+}.

Alternatively, greigite precipitation in solutions with variable saturation states may be attributed to an inorganic mechanism. Within fine grained clastic sediments, framboidal pyrite can nucleate rapidly if the diffusion of nutrients in the surrounding environment is fast (Rickard, 2019). Our iron-dominant model solutions predict that solutions are closer to saturation with respect to greigite at larger Fe/S ratios produced by the removal of sulphur by initial pyrite precipitation (Fig. 5a). This is supported by secondary greigite forming on the surface of pyrite framboids via pyrite dissolution in lacustrine and marine sediments (Wilkin and Barnes, 1997; Rowan and Roberts, 2006). Conversely, when diffusion is slow pyrite framboids may form after reaching a critical supersaturation following a lag phase (Ruiz-Agudo et al., 2014; Rickard, 2019; Thiel et al., 2019). Sulphur-dominant model solutions suggest greigite may precipitate provided $SI_{pyrite} > 0$ (Fig. 5b). Although model kinetics or fluid flow have not been incorporated, greigite precipitation at high concentrations implies these processes may occur at the mineral surface level producing high levels of supersaturation.

5. Conclusions

Reaction pathway modelling has provided constraints on the effect of iron, sulphur, pH and Eh on the formation and preservation of greigite in aqueous solutions. Modelling predictions show greigite is closer to saturation in iron-dominant solutions experiencing minor sulphur input. Greigite precipitates in solutions where $SI_{greigite} = -7$ at 25 °C. Solutions are closer to saturation with respect to greigite at temperatures below 25 °C and in solutions where $SI_{pyrite} > 0$. Altered saturation states and enrichments in iron and sulphur concentrations suggest a possible influence from microenvironments. Greigite is closer to saturation across numerous pathways using unbuffered solutions, whereas HS^- is the more favourable reactant using buffered solutions. The precipitation of greigite in highly alkaline (pH > 8) and anoxic (Eh ≤ −500 mV) unbuffered solutions indicate greigite may be preserved in conditions where polysulfides and iron hydroxides are the available reactants, possibly in non-steady state systems, such as tidal environments. These findings strengthen the perspective that greigite is more likely to precipitate and be preserved at low temperatures in the presence of pyrite. Future work in our group aims to implement the models into reactive transport codes to test further the validity of the new greigite proxy.

Declaration of Competing Interest

The authors declare that they have no known competing financial interests or personal relationships that could have appeared to influence the work reported in this paper.

Data availability

Research data associated with this article can be accessed at https://doi.org/10.5281/zenodo.7883977.

Acknowledgements

JNT is funded by an Engineering and Physical Sciences Research Council PhD scholarship (grant number: EP/T51780X/1). D. L. Parkhurst from the U.S. Geological Survey provided technical help for using PHREEQC.

Appendix A. Supplementary data

Supplementary data to this article can be found online at https://doi.org/10.1016/j.chemgeo.2023.121618.

References

Aller, R.C., 1977. The Influence of Macrobenthos on Chemical Diagenesis of Marine Sediments. Yale University, New Haven, CT, p. 600.

Anderko, A., Shuler, P.J., 1997. A computational approach to predicting the formation of iron sulfide species using stability diagrams. Comput. Geosci. 23 (6), 647–658. https://doi.org/10.1016/S0098-3004(97)00038-1.

Aubourg, C., Pozzi, J.P., Kars, M., 2012. Burial, claystones remagnetization and some consequences for magnetostratigraphy. Geol. Soc. Spec. Publ. 371 (1), 181–188. https://doi.org/10.1144/SP371.4.

Bazylinski, D.A., Frankel, R.B., Heywood, B.R., Mann, S., King, J.W., Donaghay, P.L., Hanson, A.K., 1995. Controlled Biomineralization of Magnetite (Fe3O4) and Greigite (Fe3S4) in a Magnetotactic Bacterium. Appl. Environ. Microbiol. 61 (9), 3232–3239. https://doi.org/10.1128/aem.61.9.3232-3239.1995.

Benning, L.G., Wilkin, R.T., Barnes, H.L., 2000. Reaction pathways in the Fe-S system below 100°C. Chem. Geol. 167 (1–2), 25–51. https://doi.org/10.1016/S0009-2541(99)00198-9.

Berg, J.S., Duverger, A., Cordier, L., Laberty-Robert, C., Guyot, F., Miot, J., 2020. Rapid pyritization in the presence of a sulfur/sulfate-reducing bacterial consortium. Sci. Rep. 10 (1), 1–14. https://doi.org/10.1038/s41598-020-64990-6.

Berner, R.A., 1967. Thermodynamic Stability of Sedimentary Iron Sulfides. Am. J. Sci. 265 (9), 773–785. https://doi.org/10.2475/ajs.265.9.773.

Berner, R.A., 1970. Sedimentary pyrite formation. Am. J. Sci. 268 (1), 1–23. https://doi.org/10.2475/ajs.268.1.1.

Blanchet, C.L., Thouveny, N., Vidal, L., 2009. Formation and preservation of greigite (Fe3S4) in sediments from the Santa Barbara Basin: Implications for paleoenvironmental changes during the past 35 k. Paleoceanography 24 (2). https://doi.org/10.1029/2008PA001719.

Brookins, D.G., 1988. Eh-pH Diagrams for Geochemistry. Springer-Verlag, Berlin, Heidelberg. https://doi.org/10.1007/978-3-642-73093-1_3.

Burton, E.A., Machel, H.G., Qi, J., 1993. Thermodynamic constraints on anomalous magnetization in shallow and deep hydrocarbon seepage environments. Appl. Paleomag. Sediment. Geol. 193–207 https://doi.org/10.2110/pec.93.49.0193.

Burton, E.D., Bush, R.T., Sullivan, L.A., 2006a. Acid-volatile sulfide oxidation in coastal flood plain drains: Iron-sulfur cycling and effects on water quality. Environ. Sci. Technol. 40 (4), 1217–1222. https://doi.org/10.1021/es0520058.

Burton, E.D., Bush, R.T., Sullivan, L.A., 2006b. Sedimentary iron geochemistry in acidic waterways associated with coastal lowland acid sulfate soils. Geochim. Cosmochim. Acta 70 (22), 5455–5468. https://doi.org/10.1016/j.gca.2006.08.016.

Burton, E.D., Bush, R.T., Johnston, S.G., Sullivan, L.A., Keene, A.F., 2011. Sulfur biogeochemical cycling and novel Fe-S mineralization pathways in a tidally re-flooded wetland. Geochim. Cosmochim. Acta 75 (12), 3434–3451. https://doi.org/10.1016/j.gca.2011.03.020.

Censi, P., Raso, M., Yechieli, Y., Ginat, H., Saiano, F., Zuddas, P., Brusca, L., Dalessandro, W., Inguaggiato, C., 2017. Geochemistry of Zr, Hf, and REE in a wide spectrum of Eh and water composition: the case of Dead Sea Fault system (Israel). Geochem. Geophys. Geosyst. 18, 844–854. https://doi.org/10.1002/2016GC006704.

Chase Jr., M.W., 1998. NIST-JANAF Themochemical Tables, 4th ed. J. Phys. Chem. Ref, Data, Monograph, p. 9.

Chase Jr., M.W., Davies, C.A., Downey, J.R., Frurip, D.J., McDonald, R.A., Syverud, A.N., 1995. JANAF Thermochemical Tables, 3rd ed. Am. Chem. Soc, Washington, DC.

Chen, Y., Zhang, W., Nian, X., Sun, Q., Ge, C., Hutchinson, S.M., Cheng, Q., Wang, F., Chen, J., Zhao, X., 2021. Greigite as an Indicator for salinity and sedimentation rate change: evidence from the Yangtze River Delta, China. J. Geophys. Res. Solid Earth 126 (3), 1–16. https://doi.org/10.1029/2020JB021085.

Davison, W., Phillips, N., Tabner, B., 1999. Soluble iron sulfide species in natural waters: Reappraisal of their stoichiometry and stability constants. Aquat. Sci. 61, 23–43. https://doi.org/10.1007/s000270050050.

van De Velde, S.J., Reinhard, C.T., Ridgwell, A., Meysman, F.J.R., 2020. Bistability in the redox chemistry of sediments and oceans. Proc. Natl. Acad. Sci. 117 (52), 33043–33050. https://doi.org/10.1073/pnas.2008235117.

Deng, N., Stack, A.G., Weber, J., Cao, B., de Yoreo, J.J., Hu, Y., 2019. Organic–mineral interfacial chemistry drives heterogeneous nucleation of Sr-rich (Bax, Sr1−x)SO4 from undersaturated solution. Proc. Natl. Acad. Sci. U. S. A. 116 (27), 13221–13226. https://doi.org/10.1073/pnas.1821065116.

Duverger, A., Berg, J.S., Busigny, V., Guyot, F., Bernard, S., Miot, J., 2020. Mechanisms of pyrite formation promoted by sulfate-reducing bacteria in pure culture. Front. Earth Sci. 8 (November), 1–15. https://doi.org/10.3389/feart.2020.588310.

Ferris, F.G., Fyfe, W.S., Beveridge, T.J., 1988. Metallic ion binding by Bacillus subtilis: Implications for the fossilization of microorganisms. Geology 16, 149–152. https://doi.org/10.1130/0091-7613(1988)016<0149:MIBBBS>2.3.CO;2.

Fu, Y., von Dobeneck, T., Franke, C., Heslop, D., Kasten, S., 2008. Rock magnetic identification and geochemical process models of greigite formation in Quaternary marine sediments from the Gulf of Mexico (IODP Hole U1319A). Earth Planet. Sci. Lett. 275 (3–4), 233–245. https://doi.org/10.1016/j.epsl.2008.07.034.

Gao, Y., Lesven, L., Gillan, D., Sabbe, K., Billon, G., de Galan, S., Elskens, M., Baeyens, W., Leermakers, M., 2009. Geochemical behavior of trace elements in sub-tidal marine sediments of the Belgian coast. Mar. Chem. 117 (1–4), 88–96. https://doi.org/10.1016/j.marchem.2009.05.002.

Gorlas, A., Jacquemot, P., Guigner, J.M., Gill, S., Forterre, P., Guyot, F., 2018. Greigite nanocrystals produced by hyperthermophilic archaea of Thermococcales order. PLoS One 13 (8). https://doi.org/10.1371/JOURNAL.PONE.0201549.

Gramp, J.P., Bigham, J.M., Jones, F.S., Tuovinen, O.H., 2010. Formation of Fe-sulfides in cultures of sulfate-reducing bacteria. J. Hazard. Mater. 175 (1–3), 1062–1067. https://doi.org/10.1016/j.jhazmat.2009.10.119.

Gregory, D., Meffre, S., Large, R., 2014. Comparison of metal enrichment in pyrite framboids from a metal-enriched and metal-poor Estuary. Am. Mineral. 99 (4), 633–644. https://doi.org/10.2138/am.2014.4545.

Grenthe, I., Fuger, J., Konings, J.M., Muller, A.B., Nguyen-Trung, C., Wanner, H., 1992. Chemical Thermodynamics of Uranium. NEA, OECD, Vienna.

Grønvold, F., Stølen, S., 1992. Thermodynamics of iron sulfides II. Heat capacity and thermodynamic properties of FeS and of Fe0.875S at temperatures from 298.15 K to 1000 K, of Fe0.98S from 298.15 K to 800 K, and of Fe0.89S from 298.15 K to about 650 K. Thermodynamics of formation. J. Chem. Thermodyn. 24 (9), 913–936. https://doi.org/10.1016/S0021-9614(05)80003-5.

Hartler, N., Libert, J., Teder, A., 1967. Rate of Sulfur dissolution in aqueous sodium sulfide. Indus. Eng. Chem. Proc. Design Develop. 6 (4), 398–406. https://doi.org/10.1021/i260024a002.

Hellige, K., Pollok, K., Larese-Casanova, P., Behrends, T., Peiffer, S., 2012. Pathways of ferrous iron mineral formation upon sulfidation of lepidocrocite surfaces. Geochim. Cosmochim. Acta 81, 69–81. https://doi.org/10.1016/j.gca.2011.12.014.

Helz, G.R., 2014. Activity of zero-valent sulfur in sulfidic natural waters. Geochem. Trans. 15 (1) https://doi.org/10.1186/s12932-014-0013-x.

Hoffmann, T.D., Reeksting, B.J., Gebhard, S., 2021. Bacteria-induced mineral precipitation: a mechanistic review. Microbiol. (United Kingdom) 167 (4). https://doi.org/10.1099/mic.0.001049.

Holmkvist, L., Kamyshny, A., Vogt, C., Vamvakopoulos, K., Ferdelman, T.G., Jørgensen, B.B., 2011a. Sulfate reduction below the sulfate-methane transition in Black Sea sediments. Deep-Sea Res. Part I: Oceanogr. Res. Papers 58 (5), 493–504. https://doi.org/10.1016/j.dsr.2011.02.009.

Holmkvist, L., Ferdelman, T.G., Jørgensen, B.B., 2011b. A cryptic sulfur cycle driven by iron in the methane zone of marine sediment (Aarhus Bay, Denmark). Geochim. Cosmochim. Acta 75 (12), 3581–3599. https://doi.org/10.1016/j.gca.2011.03.033.

Holmkvist, L., Kamyshny, A., Brüchert, V., Ferdelman, T.G., Jørgensen, B.B., 2014. Sulfidization of lacustrine glacial clay upon Holocene marine transgression (Arkona Basin, Baltic Sea). Geochim. Cosmochim. Acta 142 (1), 75–94. https://doi.org/10.1016/j.gca.2014.07.030.

Horng, C.S., 2018. Unusual magnetic properties of sedimentary pyrrhotite in methane seepage sediments: comparison with metamorphic pyrrhotite and sedimentary greigite. J. Geophys. Res. Solid Earth 123 (6), 4601–4617. https://doi.org/10.1002/2017JB015262.

Hunger, S., Benning, L.G., 2007. Greigite: a true intermediate on the polysulfide pathway to pyrite. Geochem. Trans. 8, 1–20. https://doi.org/10.1186/1467-4866-8-1.

Kamyshny, A., Gun, J., Rizkov, D., Voitsekovski, T., Lev, O., 2007. Equilibrium distribution of polysulfide ions in aqueous solutions at different temperatures by rapid single-phase derivatization. Environ. Sci. Technol. 41 (7), 2395–2400. https://doi.org/10.1021/es062637+.

Kamyshny, A.J., Zilberbrand, M., Ekeltchik, I., Voitsekovski, T., Gun, J., Lev, O., 2008. Speciation of polysulfides and zerovalent sulfur in sulfide-rich water wells in Southern and Central Israel. Aquat. Geochem. 14, 171–192. https://doi.org/10.1007/s10498-008-9031-6.

Kao, S.J., Horng, C.S., Roberts, A.P., Liu, K.K., 2004. Carbon-sulfur-iron relationships in sedimentary rocks from southwestern Taiwan: influence of geochemical environment on greigite and pyrrhotite formation. Chem. Geol. 203 (1–2), 153–168. https://doi.org/10.1016/j.chemgeo.2003.09.007.

Keene, A.F., Johnston, S.G., Bush, R.T., Sullivan, L.A., Burton, E.D., McElnea, A.E., Ahern, C.R., Powell, B., 2011. Effects of hyper-enriched reactive Fe on sulfidisation in a tidally inundated acid sulfate soil wetland. Biogeochemistry 103 (1), 263–279. https://doi.org/10.1007/s10533-010-9461-2.

Koretsky, C.M., van Cappellen, P., Dichristina, T.J., Kostka, J.E., Lowe, K.L., Moore, C.M., Roychoudhury, A.N., Viollier, E., 2005. Salt marsh pore water geochemistry does not correlate with microbial community structure. Estuar. Coast. Shelf Sci. 62 (1–2), 233–251. https://doi.org/10.1016/j.ecss.2004.09.001.

Kostka, J.E., Luther III, G.W., 1995. Seasonal cycling of Fe in saltmarsh sediments. Biogeochemistry 29 (2), 159–181. https://doi.org/10.1007/BF00000230.

Kuwabara, J.S., van Geen, A., McCorkle, D.C., Bernhard, J.M., 1999. Dissolved sulfide distributions in the water column and sediment pore waters of the Santa Barbara Basin. Geochim. Cosmochim. Acta 63 (15), 2199–2209. https://doi.org/10.1016/S0016-7037(99)00084-8.

LaFond-Hudson, S., Johnson, N.W., Pastor, J., Dewey, B., 2018. Iron sulfide formation on root surfaces controlled by the life cycle of wild rice (Zizania palustris). Biogeochemistry 141 (1), 95–106. https://doi.org/10.1007/s10533-018-0491-5.

Latimer, W.M., 1952. The Oxidation States of the Elements and their Potentials in Aqueous Solutions, 2nd ed. Prentice Hall, New York.

Lemire, R.J., Palmer, D.A., Taylor, P., Schlenz, H., 2020. Chemical Thermodynamics of Iron, Part 2. OECD Publishing, Paris.

Lennie, A.R., England, K.E.R., Vaughan, D.J., 1995. Transformation of synthetic mackinawite to hexagonal pyrrhotite: a kinetic study. Am. Mineral. 80 (9–10), 960–967. https://doi.org/10.2138/am-1995-9-1012.

Li, X., Cutter, G.A., Thunell, R.C., Tappa, E., Gilhooly, W.P., Lyons, T.W., Astor, Y., Scranton, M.I., 2011. Particulate sulfur species in the water column of the Cariaco Basin. Geochim. Cosmochim. Acta 75 (1), 148–163. https://doi.org/10.1016/j.gca.2010.09.039.

Lin, M.Y., Cutter, G.A., Thunell, R.C., Tappa, E., Gilhooly, W.P., Lyons, T.W., Astor, Y., Scranton, M.I., 2018. Reaction pathways of iron-sulfide mineral formation: an in situ X-ray diffraction study. Eur. J. Mineral. 30 (1), 77–84. https://doi.org/10.1127/ejm/2017/0029-2681.

Lin, S., Krause, F., Voordouw, G., 2009. Transformation of iron sulfide to greigite by nitrite produced by oil field bacteria. Appl. Microbiol. Biotechnol. 83 (2), 369–376. https://doi.org/10.1007/s00253-009-1932-9.

Liu, J., Mei, X., Shi, X., Liu, Q., Liu, Y., Ge, S., 2018. Formation and preservation of greigite (Fe3S4) in a thick sediment layer from the central South Yellow Sea. Geophys. J. Int. 213 (1), 135–146. https://doi.org/10.1093/gji/ggx556.

Liu, Y., Zhang, Z., Bhandari, N., Dai, Z., Yan, F., Ruan, G., Lu, A.Y., Deng, G., Zhang, F., Al-Saiari, H., Kan, A.T., Tomson, M.B., 2017. New approach to study iron sulfide precipitation kinetics, solubility, and phase transformation. Ind. Eng. Chem. Res. 56 (31), 9016–9027. https://doi.org/10.1021/acs.iecr.7b01615.

Luther III, G.W., 1991. Pyrite synthesis via polysulfide compounds. Geochim. Cosmochim. Acta 55, 2839–2849. https://doi.org/10.1016/0016-7037(91)90449-F.

Machel, H.G., Burton, E.A., 1991. Chemical and microbial processes causing anomalous magnetization in environments affected by hydrocarbon seepage. Geophysics 56 (5), 598–605. https://doi.org/10.1190/1.1443076.

Marnette, E.C.L., van Breemen, N., Hordijk, K.A., Cappenberg, T.E., 1993. Pyrite formation in two freshwater systems in the Netherlands. Geochem. Cosmochim. Acta 57, 4165–4177. https://doi.org/10.1016/0016-7037(93)90313-L.

Morse, J.W., Wang, Q., 1997. Pyrite formation under conditions approximating those in anoxic sediments: II. Influence of precursor iron minerals and organic matter. Mar. Chem. 57 (3–4), 187–193. https://doi.org/10.1016/S0304-4203(97)00050-9.

Neretin, L.N., Böttcher, M.E., Jørgensen, B.B., Volkov, I.I., Lüschen, H., Hilgenfeldt, K., 2004. Pyritization processes and greigite formation in the advancing sulfidization front in the upper Pleistocene sediments of the Black Sea. Geochim. Cosmochim. Acta 68 (9), 2081–2093. https://doi.org/10.1016/S0016-7037(03)00450-2.

Ning, J., Zheng, Y., Young, D., Brown, B., Nešić, S., 2014. Thermodynamic study of hydrogen sulfide corrosion of mild steel. Corrosion 70 (4), 375–389. https://doi.org/10.5006/0951.

Ning, J., Zheng, Y., Brown, B., Young, D., Nesic, S., 2015. Construction and Verification of Pourbaix Diagrams for Hydrogen Sulfide Corrosion of Mild Steel. NACE – International Corrosion Conference Series.

Nowaczyk, N.R., 2011. Dissolution of titanomagnetite and sulphidization in sediments from Lake Kinneret, Israel. Geophys. J. Int. 187 (1), 34–44. https://doi.org/10.1111/j.1365-246X.2011.05120.x.

Otero, X.L., Ferreira, T.O., Vidal-Torrado, P., Macías, F., 2006. Spatial variation in pore water geochemistry in a mangrove system (Pai Matos island, Cananeia-Brazil). Appl. Geochem. 21 (12), 2171–2186. https://doi.org/10.1016/j.apgeochem.2006.07.012.

Parkhurst, D.L., Appelo, C., 2013. Description of input and examples for PHREEQC Version 3 — A computer program for speciation, batch-reaction, one-dimensional transport, and inverse geochemical calculations. In: U.S. Geological Survey Techniques and Methods, Book 6, Chapter A43. https://doi.org/10.3133/tm6A43.

Perry, K.A., Pedersen, T.F., 1993. Sulphur speciation and pyrite formation in meromictic ex-fjords. Geochim. Cosmochim. Acta 57, 4405–4418. https://doi.org/10.1016/0016-7037(93)90491-E.

Picard, A., Gartman, A., Clarke, D.R., Girguis, P.R., 2018. Sulfate-reducing bacteria influence the nucleation and growth of mackinawite and greigite. Geochim. Cosmochim. Acta 220, 367–384. https://doi.org/10.1016/j.gca.2017.10.006.

Rickard, D., 2006. The solubility of FeS. Geochim. Cosmochim. Acta 70 (23 SPEC. ISS), 5779–5789. https://doi.org/10.1016/j.gca.2006.02.029.

Rickard, D., 2012a. Euxinic systems. In: Developments in Sedimentology. Elsevier B.V, pp. 495–542. https://doi.org/10.1016/B978-0-444-52989-3.00013-1.

Rickard, D., 2012b. Metastable sedimentary iron sulfides. In: Developments in Sedimentology. Elsevier B.V, pp. 195–231. https://doi.org/10.1016/B978-0-444-52989-3.00005-2.

Rickard, D., 2019. How long does it take a pyrite framboid to form? Earth Planet. Sci. Lett. 513, 64–68. https://doi.org/10.1016/j.epsl.2019.02.019.

Rickard, D., Luther, G.W., 2007. Chemistry of iron sulfides. Chem. Rev. 107 (2), 514–562. https://doi.org/10.1021/cr0503658.

Rickard, D., Morse, J.W., 2005. Acid volatile sulfide (AVS). Mar. Chem. 97, 141–197. https://doi.org/10.1016/j.marchem.2005.08.004.

Rickard, D., Butler, I.B., Oldroyd, A., 2001. A novel iron sulphide mineral switch and its implications for Earth and planetary science. Earth Planet. Sci. Lett. 189, 85–91. https://doi.org/10.1016/S0012-821X(01)00352-1.

Roberts, A.P., 1995. Magnetic properties of sedimentary greigite (Fe3S4). Earth Planet. Sci. Lett. 134 (3–4), 227–236. https://doi.org/10.1016/0012-821X(95)00131-U.

Roberts, A.P., 2015. Magnetic mineral diagenesis. Earth Sci. Rev. 151, 1–47. https://doi.org/10.1016/j.earscirev.2015.09.010.

Roberts, A.P., Turner, G.M., 1993. Diagenetic formation of ferrimagnetic iron sulphide minerals in rapidly deposited marine sediments, South Island, New Zealand. Earth Planet. Sci. Lett. 115, 257–273. https://doi.org/10.1016/0012-821X(93)90226-Y.

Roberts, A.P., Weaver, R., 2005. Multiple mechanisms of remagnetization involving sedimentary greigite (Fe3S4). Earth Planet. Sci. Lett. 231 (3–4), 263–277. https://doi.org/10.1016/j.epsl.2004.11.024.

Roberts, A.P., Reynolds, R.L., Verosub, K.L., Adam, D.P., 1996. Environmental magnetic implications of greigite (Fe3S4) formation in a 3 m.y. lake sediment record from Butte Valley, northern California Andrew. Geophys. Res. Lett. 23 (20), 2859–2862. https://doi.org/10.1029/96GL02831.

Robie, R.A., 1966. Thermodynamic properties of minerals. In: Clark, S.P. (Ed.), Handbook of Physical Constants. Geological Society of America Inc., New York, pp. 437–458. https://doi.org/10.1130/MEM97-p437.

Robie, R.A., Hemingway, B.S., 1995. Thermodynamic Properties of Minerals and Related Substances at 298.15 K and 1 Bar (10^5 Pascals) Pressure and at Higher Temperatures. USGS, Washington, D.C.. https://doi.org/10.3133/b2131

Rowan, C.J., Roberts, A.P., 2005. Tectonic and geochronological implications of variably timed magnetizations carried by authigenic greigite in marine sediments from New Zealand. Geology 33 (7), 553–556. https://doi.org/10.1130/G21382.1.

Rowan, C.J., Roberts, A.P., 2006. Magnetite dissolution, diachronous greigite formation, and secondary magnetizations from pyrite oxidation: Unravelling complex magnetizations in Neogene marine sediments from New Zealand. Earth Planet. Sci. Lett. 241 (1–2), 119–137. https://doi.org/10.1016/j.epsl.2005.10.017.

Rudmin, M., Roberts, A.P., Horng, C.S., Mazurov, A., Savinova, O., Ruban, A., Kashapov, R., Veklich, M., 2018. Ferrimagnetic iron sulfide formation and methane venting across the paleocene-eocene thermal maximum in shallow marine sediments, ancient West Siberian Sea. Geochem. Geophys. Geosyst. 19 (1), 21–42. https://doi.org/10.1002/2017GC007208.

Rudmin, M., Mazurov, A., Banerjee, S., 2019. Origin of ooidal ironstones in relation to warming events: Cretaceous-Eocene Bakchar deposit, south-East Western Siberia. Mar. Pet. Geol. 100, 309–325. https://doi.org/10.1016/j.marpetgeo.2018.11.023.

Ruiz-Agudo, E., Putnis, C.V., Putnis, A., 2014. Coupled dissolution and precipitation at mineral-fluid interfaces. Chem. Geol. 383, 132–146. https://doi.org/10.1016/j.chemgeo.2014.06.007.

Schoonen, M.A.A., Barnes, H.L., 1991. Reactions forming pyrite and marcasite from solution: I. Nucleation of FeS2 below 100°C. Geochim. Cosmochim. Acta 55 (6), 1495–1504. https://doi.org/10.1016/0016-7037(91)90122-L.

Schultze-Lam, S., Fortin, D., Davis, B.S., Beveridge, T.J., 1996. Mineralization of bacterial surfaces. Chem. Geol. 132, 171–181. https://doi.org/10.1016/S0009-2541(96)00053-8.

Shumway, S.G., Wilson, J., Lilova, K., Subramani, T., Navrotsky, A., Woodfield, B.F., 2022. The low-temperature heat capacity and thermodynamic properties of greigite (Fe3S4). J. Chem. Thermodyn. 173 https://doi.org/10.1016/j.jct.2022.106836.

Silva-Castro, G.A., Uad, I., Rivadeneyra, A., Vilchez, J.I., Martin-Ramos, D., González-López, J., Rivadeneyra, M.A., 2013. Carbonate Precipitation of Bacterial Strains Isolated from Sediments and Seawater: Formation Mechanisms. Geomicrobiol J. 30 (9), 840–850. https://doi.org/10.1080/01490451.2013.777492.

Snowball, I., Thompson, R., 1988. The occurrence of Greigite in sediments from Loch Lomond. J. Quat. Sci. 3 (2), 121–125. https://doi.org/10.1002/jqs.3390030203.

Son, S., Pil Hyun, S., Charlet, L., Kwon, K.D., 2022. Thermodynamic stability reversal of iron sulfides at the nanoscale: Insights into the iron sulfide formation in low-temperature aqueous solution. Geochim. Cosmochim. Acta. https://doi.org/10.1016/j.gca.2022.10.021.

Steefel, C.I., Appelo, C.A.J., Arora, B., Jacques, D., Kalbacher, T., Kolditz, O., Lagneau, V., Lichtner, P.C., Mayer, K.U., Meeussen, J.C.L., Molins, S., Moulton, D., Shao, H., Šimůnek, J., Spycher, N., Yabusaki, S.B., Yeh, G.T., 2015. Reactive transport codes for subsurface environmental simulation. Comput. Geosci. 19 (3), 445–478. https://doi.org/10.1007/s10596-014-9443-x.

Subramani, T., Lilova, K., Abramchuk, M., Leinenweber, K.D., Navrotsky, A., 2020. Greigite (Fe3S4) is thermodynamically stable: Implications for its terrestrial and planetary occurrence. Proc. Natl. Acad. Sci. U. S. A. 117 (46), 28645–28648. https://doi.org/10.1073/pnas.2017312117.

Sweeney, R.E., Kaplan, I.R., 1973. Pyrite framboid formation: laboratory synthesis and marine sediments. Econ. Geol. 68, 618–634. https://doi.org/10.2113/gsecongeo.68.5.618.

Thiel, J., Byrne, J.M., Kappler, A., Schink, B., Pester, M., 2019. Pyrite formation from FeS and H 2 S is mediated through microbial redox activity. Proc. Natl. Acad. Sci. U. S. A. 116 (14), 6897–6902. https://doi.org/10.1073/pnas.1814412116.

Wada, H., 1977. The synthesis of greigite from a polysulfide solution at about 100°C. Bull. Chem. Soc. Jpn. 50, 2615–2617. https://doi.org/10.1246/bcsj.50.2615.

Wan, M., Shchukarev, A., Lohmayer, R., Planer-Friedrich, B., Peiffer, S., 2014. Occurrence of surface polysulfides during the interaction between ferric (Hydr) oxides and aqueous sulfide. Environ. Sci. Technol. 48 (9), 5076–5084. https://doi.org/10.1021/es405612f.

White, L.M., Bhartia, R., Stucky, G.D., Kanik, I., Russell, M.J., 2015. Mackinawite and greigite in ancient alkaline hydrothermal chimneys: identifying potential key catalysts for emergent life. Earth Planet. Sci. Lett. 430, 105–114. https://doi.org/10.1016/j.epsl.2015.08.013.

Wilkin, R.T., Barnes, H.L., 1996. Pyrite formation by reactions of iron monosulfides with dissolved inorganic and organic sulfur species. Geochim. Cosmochim. Acta 60 (21), 4167–4179. https://doi.org/10.1016/S0016-7037(97)81466-4.

Wilkin, R.T., Barnes, H.L., 1997. Formation processes of framboidal pyrite. Geochim. Cosmochim. Acta 61 (2), 323–339. https://doi.org/10.1016/S0016-7037(96)00320-1.

Wilkin, R.T., Ford, R., 2006. Arsenic solid-phase partitioning in reducing sediments of a contaminated wetland. Chem. Geol. 228, 156–174. https://doi.org/10.1016/j.chemgeo.2005.11.022.

Wong, V.N.L., Johnston, S.G., Burton, E.D., Bush, R.T., Sullivan, L.A., Slavich, P.G., 2013. Seawater-induced mobilization of trace metals from mackinawite-rich estuarine sediments. Water Res. 47 (2), 821–832. https://doi.org/10.1016/j.watres.2012.11.009.

Xu, F., Navrtosky, A., 2010. Enthalpies of formation of pyrrhotite $Fe_{1-0.125x}S$ ($0 \leq x \leq 1$) solid solutions. American Mineralogist 95 (5–6), 717–723. https://doi.org/10.2138/am.2010.3334.

Yang, T., Dekkers, M.J., Zhao, X., Petronotis, K.E., Chou, Y., 2022. Greigite formation modulated by turbidites and bioturbation in deep-sea sediments offshore Sumatra. J. Geophys. Res. Solid Earth 127. https://doi.org/10.1029/2022JB024734.